N O T I C E

THIS DOCUMENT HAS BEEN REPRODUCED FROM MICROFICHE. ALTHOUGH IT IS RECOGNIZED THAT CERTAIN PORTIONS ARE ILLEGIBLE, IT IS BEING RELEASED IN THE INTEREST OF MAKING AVAILABLE AS MUCH INFORMATION AS POSSIBLE

NASA

Technical Memorandum 80643

A Solar Extreme Ultraviolet Telescope and Spectrograph for Space Shuttle
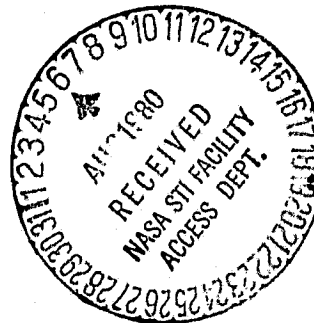
Volume I
Investigation and Technical Plan

NOVEMBER 1978

National Aeronautics and
Space Administration

Goddard Space Flight Center
Greenbelt, Maryland 20771

VOL. I

INVESTIGATION AND TECHNICAL PLAN

A SOLAR EXTREME ULTRAVIOLET TELESCOPE AND SPECTROGRAPH FOR SHUTTLE

NOVEMBER 1978

Primary Discipline: Solar Physics

Principal Investigator:

>Dr. Werner M. Neupert
>Laboratory for Astronomy and Solar Physics
>Code 682
>Goddard Space Flight Center
>Greenbelt, MD 20771
>Telephone: 301-982-5523

Co-Investigators:

Naval Research Laboratory
Washington, D.C. 20390

Dr. Uri Feldman
Code 7147
Telephone: 202-767-2718

Laboratory for Astronomy and Solar Physics
Goddard Space Flight Center
Greenbelt, MD 20771

Dr. Robert D. Chapman
Code 680
Telephone: 301-982-5101

Dr. Gabriel L. Epstein
Code 682
Telephone: 301-982-5616

Dr. James A. Ionson
Code 682
Telephone: 301-982-6184

Dr. Andrew Michalitsianos
Code 684
Telephone: 301-982-6177

Dr. Roger J. Thomas
Code 682
Telephone: 301-982-4914

TABLE OF CONTENTS

I. SUMMARY OF INVESTIGATION

This proposal outlines a scientific investigation that addresses several fundamental problems of solar physics:

o The energy and mass balances in closed magnetic field regions in the corona and the processes by which these regions are heated.

o Mass and energy transport into the solar wind.

o The characteristics of the emergence and evolution of coronal active regions and their relation to flare activity and coronal holes.

An investigation of these problems requires observations with high spectral resolution simultaneously over the range of solar temperatures from 1×10^5 to 2×10^7K, and over an extended field of view. The required observations are most effectively obtained in the extreme ultraviolet but no adequate data have been obtained to date. No instrument available on the Solar Maximum Mission or currently being developed for Spacelab 1 or 2 can make such measurements. Thus, we propose to construct and use a solar extreme ultraviolet telescope and spectrograph (SEUTS) for the Spacelab program.

The instrument proposed is a novel combination of existing technologies that most effectively provides the needed EUV data. A grazing incidence telescope with high EUV reflectivity feeds a diffraction grating at near normal incidence. The grating, ruled on a toroidal surface, not only spectrally disperses the radiation but also images each point of the spectrometer's entrance aperture onto a small spot in the focal plane so that spatial information is preserved. Adequately stigmatic images are produced over an 8 arcmin long slit and over a spectral range of 22.5 to 37.0nm. This is the most effective, narrow range of wavelengths containing emission lines sensitive to the temperature range that must be observed. Schumann-type photographic film is used to gain the full performance of the optical system. Spatial resolution of at least 2 arcsec and spectral resolution of 0.005nm is achievable throughout the central 4 arcmin field of view at all wavelengths with even better performance in the Rowland plane.

Recognizing that rapid solar phenomena cannot be fully investigated with a footage-limited film system, we also propose to carry and operate an open-mesh photocathode intensified CCD detector for engineering evaluation on the first flight. This offers an opportunity to evaluate such parameters as operation (and possible degradation) in the orbiter environment, detector stability during the extended integration period and sensitivity to the high energy particle environment of the orbiter. Observations will be made over a restricted wavelength range of 33.5 - 35.7nm and results will guide more extended use of such detectors in the prime focal plane on future missions.

II. SCIENTIFIC BASIS AND OBJECTIVES

A. Introduction

Observations of the past decade have fundamentally changed our understanding of the physical processes in the solar corona. They have demonstrated the profound role that magnetic fields play in defining coronal structures,

controlling transport of mass and energy in the sun's atmosphere, and, ultimately, determining the state of the interplanetary plasma within which the earth moves. We are now also much more aware of the dynamic nature of the corona as illustrated by coronal transients, rapid loop brightenings and fadings, and the coronal components of solar flares.

In the past ten years we have moved from space observations that gave only the barest information on the spatial distribution of radiation to observations on the level of 1 arcsec in ultraviolet wavelengths (> 120 nm) and ~ 5 arcsec at extreme ultraviolet wavelengths. Instruments now planned for Spacelab 2 will extend ultraviolet observations in resolution and show us the time development of magnetically controlled structures in the chromosphere and lower transition zone (T_e < 200,000K). Nonetheless, the OSO and ATM workshops of the past several years have shown that our knowledge of the corona's physical properties and our data base are too inadequate to discriminate among various theories for the heating of active regions, the triggering and energy conversion and dissipation in flares, and the sources of energy to drive the solar wind.

With the instruments now being built we will obtain only glimpses, using one or two weak forbidden lines, of the coronal counterparts of low temperature phenomena. What is now vitally needed is corresponding instrumentation that will perform the same detailed studies of the corona as are now planned for the chromosphere and transition zone. Such comprehensive work can best be carried out at extreme ultraviolet (EUV) wavelengths where the strongest emission lines of highly stripped ions are located.

We now have diagnostic techniques for inferring coronal electron densities which, together with observed emission measures, allow us to estimate sizes of features that may lie below the limit of resolution of our instrumentation. Such information, coupled with data on turbulent and directed plasma motions derived from line profiles, can provide critical tests of theories of active region heating, models of solar wind acceleration, and concepts of flare energy release mechanisms. No instrument is available on SMM or is currently being developed for Spacelab 1 or 2 to make such measurements in the solar corona.

Our prime scientific objectives require EUV observations with high spectral ($\Delta\lambda \approx 0.005nm$) and spatial ($\Delta s \approx 2$ arcsec) resolution simultaneously over a wide range of solar temperatures ($1 \times 10^5 - 2 \times 10^7$K) and over an extended field of view. We intend to:

1) Observe emission line profiles and intensities over a wide range of transition zone and coronal temperatures for many types of features (active regions, quiet sun, coronal holes, etc.) in order to correlate turbulent and directed mass flows with the coronal conditions of electron temperature and density in which they are found.

2) Search for periodic and aperiodic (possibly impulsive) intensity variations of spectral lines as a function of temperature that may be indicative of wave processes or other forms of energy injection into the corona.

3)   Observe coronal and transition zone loop configurations and their changes prior to and following flares to assess the role that coronal magnetic fields and their possible instabilities play in the flare phenomenon.

4)   Observe the EUV line emission of flares as a means of identifying the locations of impulsive components, sources of mass for the high temperature plasma and processes by which energy is converted and dissipated during the flare event.

In the following pages we discuss the need for coronal observations and then present the instrument that we propose to build and operate on the Shuttle/Spacelab.

B.   Active Regions

Spatially resolved observations in both X-rays and EUV from rockets, the Skylab, and the OSO satellites have demonstrated that the active region corona consists principally of magnetically confined plasmas whose enchanced emission reflects enhanced energy dissipation within the enclosed structures.[1-5] To understand the physical processes governing these loops, we must answer certain key questions:

1)   What is the energy source that sustains them against radiation and conduction losses?

2)   How is energy extracted from this source and subsequently converted into kinetic energy (i.e., heat)?

3)   What mechanisms govern the transport of "heat" within and between loops?

The two most likely candidates for transporting energy into a loop are a) electric currents, both D.C.[6] and A.C.[7,8] (i.e., hydromagnetic body waves) and b) surface waves.[9] In both cases energy is stored in the form of non-potential magnetic fields and irreversibly converted into "heat" by some combination of classical[10] or anomalous[6] Joule dissipation, wave-wave interactions,[7,8] resonant absorption,[9] and magnetohydrodynamic tearing instabilities.[11,12]

In light of the extremely efficient thermal conduction along magnetic field lines (which presumably define the loops), heating distributions as disparate as uniform input along the loop and a delta function input at the top probably have indistinguishable steady-state radiation signatures. We must, therefore, look to the radial, temporal, and spectral manifestations of loops' spatial inhomogeneities to evaluate the various loop models. For instance, D. C. Joule heating may occur as localized heating pulses where magnetic field instabilities appear, producing short-lived (a few seconds) hot spots in a loop. Alfvenic surface waves, on the other hand, would lead to a relatively constant, hot sheath surrounding cooler material.

Data with 2 arcsec resolution from the SEUTS would be a significant improvement over the 5 arcsec EUV data currently available to test and develop theories. The 2 arcsec resolution may be sufficient to define the spatial and temporal behavior of a loop's footpoints precisely enough to determine

the dominant heating mechanism. D.C. Joule heating is characterized by differential twisting of the footpoints while hydromagnetic wave heating requires a relatively more coherent shaking of them.

Even 2 arcsec resolution, however, will be inadequate to resolve the radial structures called for by current theories[9,13] in which thermodynamic variation occurs over tens or hundreds of kilometers. To search for spatial inhomogeneities and kinematic variations in loops that could be used to test these theories, we will turn to spectral diagnostic techniques. Electron density sensitive line ratios would reveal the former, while observation of emission line broadening and Doppler shifts would give evidence of turbulence and mass flows, delineating the latter.

For example, Ionson's loop model,[9] based on excitation of Alfvénic surface waves (300 second period, 8 km/s velocity amplitude), predicts hot (2.9×10^6K), fast upflows (10-100 km/s) within a boundary layer (≤ 100 km thick) between a thin (≤ 1 km), irreversibly heated sheath and cool ($\gtrsim 10^4$K) downflowing (< 100 km/s) plasma in the loops's core. Such flows would be easily detected as line shifts in an axial loop observation made with our instrument, even though the radial variations could not be spatially resolved.

So far we have discussed only the physics of individual loops. To fully understand active regions we must also study the coupling between individual loops and the properties of the coronal plasma as it may exist outside the prominent loop structures. For all these studies, as for coronal bright points, the SEUTS, covering a wide range of coronal and transition zone temperatures and working with other instruments probing the photosphere and chromosphere on the same space mission, would be a very powerful tool.

C.   Coronal Holes

A major result of the solar space program has been the discovery and investigation of coronal holes--regions of diminished density and temperature in the corona that are the sources of recurrent high-speed wind streams[4] and are strongly correlated with geomagnetic phenomena[15]. Initial models emphasized the lowered temperature and density in coronal holes as compared to surrounding areas of the quiet sun and the fact that coronal holes had an open magnetic topology characterized by a supra-radial expansion of the field into interplanetary space[16-18].

Recently, a number of hydromagnetic coronal hole models have emerged[19-22] that begin to address their plasma dynamics as well as their temperature-density structure. However, the measurements of the upper transition zone/lower corona (≤ 1.1 $R_\odot$), on which the models are based in part, need refining and verification. For example, the electron densities used are based either on extrapolation of coronagraph observations made at large radial heights above the solar limb or on models constructed from EUV line intensities and assumptions such as hydrostatic equilibrium[18]. Furthermore, although recent results suggest that the magnetic topology has important implications for the wind stream dynamics, none of the models can explain the extremely high velocity wind streams.

Thus, a major unsolved problem in modeling coronal holes is the connection between energy deposition and acceleration of high-speed streams. Two likely

energy deposition mechanisms are <u>in situ</u> heating of plasma via current dissipation (e.g., magnetic field annihilation) and hydromagnetic wave dissipation. The latter is particularly attractive because, in addition to a heat-generated gas pressure gradient, there exists a gradient in the wave momentum flux further accelerating the coronal hole plasma.

Most proposed heating and acceleration mechanisms are inherently nonuniform. It is essential, therefore, to make two-dimensional (i.e., "above" and "along" the solar disk) observations of the coronal hole parameters. One such parameter, sensitive to energy deposition, is the nonthermal broadening of spectral lines. In the transition zone it increases with increasing temperature of line formation. However, very little is known about its behavior in the upper transition zone/lower corona. The few observations made suggest that random mass motions are somewhat smaller in the corona than in the transition zone. Data from SEUTS will allow a detailed examination of nonthermal mass motions up into the corona, providing powerful constraints on theories treating the heating of these layers in coronal holes.

Current theories and empirical models of the important inner corona, and one suggestive observation,[23,24] indicate the presence of mass flows of from 10 to 20 km/s in coronal holes at heights where the temperature reaches about 10^6K. Confirmation of Doppler shifts in lines formed in this temperature regime would be direct evidence of such flows and provide an observational determination of where and at what level in the coronal hole the solar wind acceleration takes place. This information, together with a more precise empirical temperature-density model of the vital upper transition zone/lower corona, would be a stringent bound for any proposed acceleration mechanism. The SEUTS can provide both the line profile data and emission line intensities that are needed to develop more sophisticated models of coronal holes.

D.   The Quiet Sun

Before this decade it was reasonable to talk of a "quiet" solar atmosphere composed of concentric, homogeneous layers differing in temperature, density, and thickness, embedded in which were, e.g., active regions and prominences. However, investigations with instruments on Skylab, OSO's, and rockets have shown that inhomogeneity is the rule, not the exception.

Away from active regions and outside coronal holes, the primary structural elements of the corona appear to be loops,[25,26] similar to those in active regions but closed on a larger scale (~ 0.5 $R_\odot$) and somewhat more ordered. Whether these "quiet" coronal loops are structurally different from the active region loops and whether they are powered and maintained by different physical processes are unanswered questions. Thus far instruments have lacked the spectral and spatial capabilities to determine the structural and dynamical properties of individual loops. The NRL HRTS has come closest, but can only provide glimpses of the corona in one or two weak forbidden lines.[27] A major observational effort with an analogous instrument is required to get the EUV emission line characteristics of these hugh "quiet" coronal structures.

No definitive evidence for periodic intensity fluctuations in the quiet corona has ever been found. However, Skylab investigators have seen short-lived

aperiodic pulses of ultraviolet emission[28] suggesting energy carried upward in shockwaves. In addition, observations of transition zone lines with the stigmatic HRTS[27] reveal jets of high density material surging upward in the chromospheric network and in active regions. It has been suggested that these jets may be responsible for a momentum-driven solar wind where the energy is injected at the solar surface. This hypothesis can be verified with the SEUTS, which will be capable of tracing such jets from the lower transition zone to higher, coronal levels. To correlate the SEUTS observations with those in the strong C IV 155 nm line (in which the jets have been seen) we propose coordinated observation with the Spacelab HRTS.

In the case of the quiet sun transition zone, mean models were justified in spite of obvious inhomogeneities (e.g , network and spicules) because physical conditions appeared to be fairly constant from one region to another. However, the balance between mechanical energy deposition in the lower corona and radiative and conductive fluxes down through the transition zone is highly sensitive to the assumed distribution of material within a resolution element.[29,30]

For example, the transition zone temperature gradient derived from $\geq$ 5 arcsec observations is incompatible with the observed intensity of the He I and He II resonance lines.[31] Calculations using that gradient show that absorption of coronal, ionizing photons by He II ions is very inefficient.[32] Yet painstaking measurement of NRL Skylab spectroheliograms suggest that He II 25.6 nm is formed primarily by photoionization-recombination.[33] The picture is further confused by the tremendous contrast across the solar surface displayed by the optically thin He II 164 nm multiplet.[27] Stigmatic spectra taken with the SEUTS, in coordination with NRL Spacelab HRTS observations of the 164 nm multiplet, would be a tremendous aid in interpreting the He II quiet sun spectrum.[34-36]

Exhaustive investigations with OSO-8[37,38] show that while there are no strong periodicities on average in either the intensity or velocity field at the level of the Si IV and C IV lines, there is an indication of downward propagating 300 s waves. Coupling this with the weak evidence of 300 s oscillations in He II 30.4 nm[39] we propose to look again at that line with an instrument providing better spectral and spatial resolution.

Since gas pressures within quiescent prominences are less than the ambient coronal pressures, they would appear to get most of their support from magnetic fields. Measurements of electron temperatures and densities using intensity ratios of lines with temperatures of formation under 10^6K will clarify the field strengths required. The pressure distribution within a prominence is governed by its structure which probably consists of many cylindrical threads of material. These threads may have internal structure like coronal loops, and a full study of them will probably require sub-arcsec resolution. Nonetheless, it should be possible to determine whether high temperature material sheaths each thread or only the prominence as a whole.

E.   Flares and Associated Phenomena

Solar flares produce such a wealth and diversity of phenomena that their study will undoubtedly prove fruitful for many years to come, even beyond the

concerted effort being mounted by the Solar Maximum Mission. In fact, the instrument proposed here will provide information unavailable from SMM which, unfortunately, will not include an EUV spectroheliograph. As described earlier, the SEUTS is a powerful probe of the corona, now thought to be the location of most of the important physical processes prior to and after the initial phases of a flare event, and likely the site of the flare initiation itself.

Virtually all recent analyses of the XUV emission associate. /ith solar flares[40-43] have shown that the plasma cannot be characterized by a single electron temperature at any time in its evolution. A continuous range of temperatures, from chromospheric to as high as 40×10^6K, must exist simultaneously within the flaring volume. Thus, measurements need to be made over this entire range with high "temperature resolution" in order to determine adequately the actual temperature and density distributions of the XUV emitting material. At the same time, very high spatial resolution is required since the scale of basic flare structures appears to be small. Flare loops have characteristic dimensions of only a few arcsec, at least for the relatively minor events recorded by Skylab.

Herein lies the basic strength of the measurement technique we propose: simultaneous observations of flare emission with two-arcsec resolution at several selected wavelengths will allow us to precisely determine the temperature and density structure of the flare as a function of position. The wavelength range from 22.5 to 37.0 nm not only contains ample coronal diagnostics, but also many flare diagnostics.[44-46]

The types of measurements just described can make significant contributions to several fundamental areas of flare research such as:

> Preflare configuration (Shear vs. height; twisted flux tubes)
> Existence of flare trigger and/or precursors
> Site of flare onset
> Relative roles of radiative and conductive cooling
> Location and duration of energy input
> Coronal counterpart to chromospheric (Hα, He I, and He II) flare kernals
> Flare oscillations
> Post-flare relaxation of coronal magnetic fields
> Structure and energetics ₒf post-flare loops

Because the early Shuttle missions will be too short to ensure adequate coverage of flare events these studies will not be our highest priority. However, the design of the SEUTS instrument and our mission plans will allow us to take advantage of opportunities to observe flares and other transient events should they occur.

III. INVESTIGATIVE APPROACH

A. Experiment Rationale

There are two main scientific reasons for selecting the region between 22.5 and 37.0 nm for high spatial and spectral resolution observations: first, the presence of spectral lines spanning a very wide range of temperatures, from lower transition zone (e.g., He II 30.4 nm) up to coronal flare temperatures (e.g., Fe XXIV 25.5 nm and Ni XXVI 23.4 nm); and second, the availability

of many spectroscopic diagnostics that will allow determination of electron
density, differential emission measures, mass flows, and nonthermal random mass
motions ("turbulence") of many solar features that extend into the corona.
m
Examples of the many different kinds of lines emitted between 22.5 and 37.0 nm
are given in Appendix AI. Lines of He II, C IV, N IV, O IV, and O V are
emitted at lower transition-zone temperature. The upper transition zone emits
lines of Mg VI--Mg VIII. The quiet corona can be studied in lines of Si IX--
Si XI, Fe IX--Fe XIV, and S XII. Active regions are represented by lines of
S XIII, Fe XV, Fe XVI, and Ni XVIII. During solar flares, lines of Ca XVIII,
Fe XXI--Fe XXIV, and Ni XXVI appear strongly. Every region of the solar
atmosphere above 2×10^4K can be studied in the narrow 22.5 to 37.0 nm range,
thereby obtaining uniformly good optical performance over the entire wavelength
band, conserving precious film, and providing the data for inflight calibration.

Numerous spectroscopic diagnostics have been developed in recent years for
determining the electron density in different regions of the solar atmosphere.[1-3]
To illustrate the intensity variations with density that may be observed, we
have prepared a synthetic spectrum Appendix AII) using the best known spectro-
scopic and atomic physics information. The intensities of strong resonance
lines can be used to derive differential emission measures in the usual way.
With the simultaneous high spatial and spectral resolution that the SEUTS will
deliver, the line profiles will give the mass flows and random mass motions
of solar plasmas through Doppler shifts and Doppler broadenings. The spatial
and spectral capabilities of our instrument, together with the ability to
observe high temperature lines (e.g., Ni XXVI 23.4 nm, Fe XXIV 25.5 nm,
and Fe XXIII 26.3 nm) will permit us to define the temperature-density structure
of flare loops.

B.   Selection of the Experimental Technique

In selecting the appropriate technique to achieve the stated scientific objectives
and take advantage of the diagnostic capabilities available at extreme ultra-
violet wavelengths, our criteria are:

1)   Observe simultaneously the intensities and profiles of a number of
spectral lines representing emission from a wide range of temperatures.

2)   Observe simultaneously a number of adjacent spatial elements. Such
observations will allow us to explore the spatial coherence or propagation
of phenomena that may be found.

3)   Use currently available techniques that can be readily adapted to
the interfaces and operational capability being provided.

Fully grazing incidence systems such as that flown by Goddard Space Flight
Center on OSO-7 provide high efficiency and the capability of recording several
emission lines simultaneously. However, no grazing incidence grating design
can be made even approximately stigmatic over the required wavelengths so con-
dition (2) cannot be satisfied. While designs using fully normal incidence
optics can be made stigmatic[4,5], those with two or more reflections have such
low efficiency below 40 nm that the number of emission lines available for
diagnostic purposes is reduced to an unacceptably low figure. Those using
only one near-normal incidence reflection[6,7] produce overlapping solar images

in the many EUV lines whose emission is distributed over the solar disk, thus reducing the recorded contrast; they also do not provide unambiguous line-profile information.
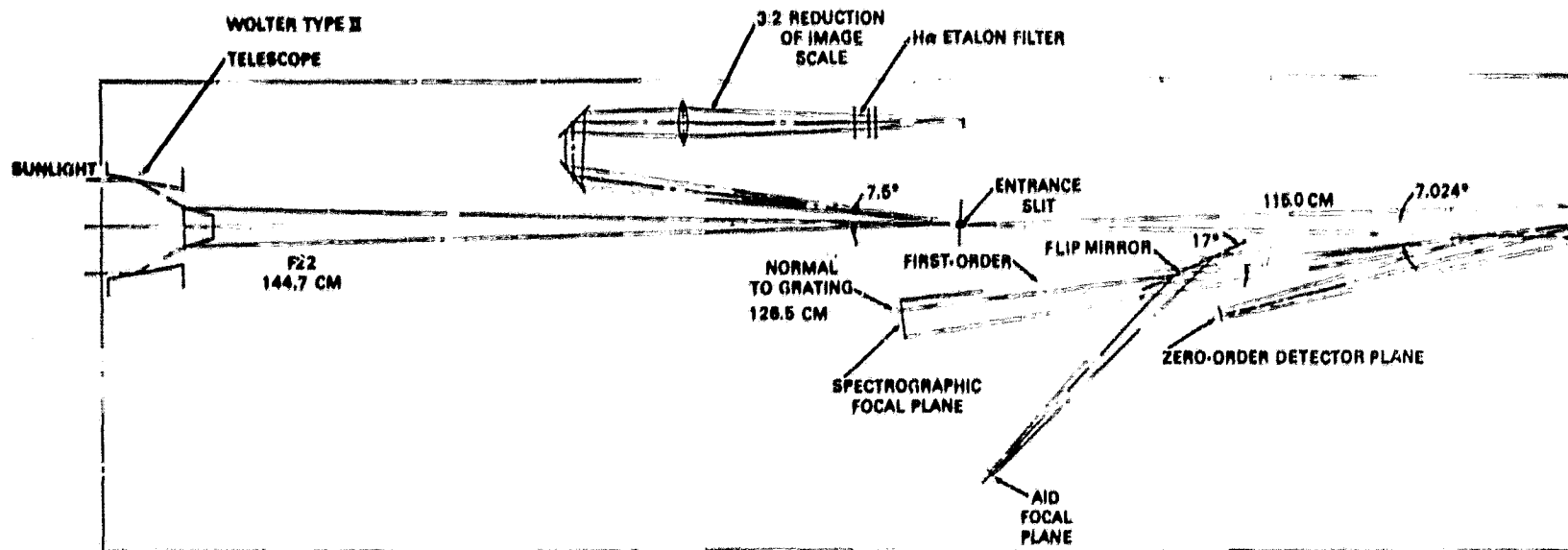
Our solution to these difficulties is to combine a Wolter Type II grazing incidence telescope having high EUV reflectivity with an aspheric near-normal incidence grating system which produces approximately stigmatic images of the solar image at each wavelength. A slit placed at the focus of the telescope simultaneously acts as the entrance aperture for the spectrograph and defines the array of spatial elements that will be refocussed, at each wavelength, in the final focal plane. This optical design also provides a flexible data format (via commandable selection of one of four entrance apertures) that can be employed to optimize scientific observing programs. The present design incorporates:

1) A line profile mode ($\Delta\lambda \approx 0.004 - 0.005$ nm) yielding stigmatic spectra over a geometric field of view (FOV) of 0.5 arcsec x 8 arcmin. In this mode the SEUTS will produce spectra from 22.5 to 37.0 nm with spectral and spatial properties similar to the spectra produced by the HRTS from 117 to 172 nm.

2) A "non-overlapping" spectroheliogram mode with a 0.3 x 8 arcmin FOV for many strong lines. The slit width (0.3 arcmin) corresponds to about 0.1 nm. Spectrally non-overlapping solar images can be built up simultaneously in many strong lines by displacing the pointing direction 0.3 arcmin between observations.

3) A combination mode providing mode 2 spectroheliograms over most of a 0.3 x 8 arcmin FOV but with mode 1 line profile observations in the central (0.5 arcsec wide by 0.8 arcmin long) portion of the field.

4) A wide field mode (5 x 8 arcmin FOV) for flare studies, with spatial resolution in the direction of dispersion governed by the Doppler widths of the spectral lines. In this mode, the instrument is similar to the SO82A slitless spectrograph on Skylab.

C.   Instrument Description

1.   Introduction

The SEUTS consists of one primary optical system for EUV wavelengths together with an H-alpha slit-jaw monitor and an EUV exposure meter that, respectively, facilitate the selection of targets and the optimization of exposure times. The principal optical paths can be traced in Figure 1. Incident radiation is focussed by grazing incidence optics onto a focal plane where a solar image is formed. A portion of the solar disc is selected, using an aperture in this focal plane, and admitted to illuminate a toroidal grating. The grating is designed not only to disperse this radiation but also to image each point on the entrance aperture onto a point in the focal plane so that spatial information is preserved. A portion of the solar image not admitted to the grating is reflected to an Hα video monitor to provide target selection and context for comparison with ground-based data. The radiation reflected at zero order from the grating is intercepted by an EUV-sensitive photoelectric detector (identical to those used on OSO-3,5 and 7) whose output is read on engineering data lines, thus permitting optimum selection of exposure times. Photographic film has been selected for prime scientific data because it can

WOLTER TYPE II
TELESCOPE

3:2 REDUCTION OF IMAGE SCALE

Hα ETALON FILTER

SUNLIGHT

F22
144.7 CM

7.5°

NORMAL TO GRATING
126.5 CM

ENTRANCE SLIT

FIRST-ORDER

FLIP MIRROR

17°

115.0 CM

7.024°

SPECTROGRAPHIC FOCAL PLANE

ZERO-ORDER DETECTOR PLANE

AID FOCAL PLANE

OPTICAL LAYOUT OF SEUTS

TELESCOPE

TOROIDAL GRATING

TECTOR PLANE

CM   7.024°

TOROIDAL GRATING

Hα ETALON FILTER

SLIT JAW CAMERA

ENTRANCE SLIT

SHUTTER

PICKOFF MIRROR

LENS

EXPOSURE METER

TELESCOPE

HEAT REJECTOR

FILM CAMERA

AID

EGG-CRATE BASEPLATE

ISOMETRIC OF SEUTS

DIRECTION OF MOTION

Fig. 1

TOROIDAL
GRATING

DIRECTION
OF MOTION

CAS

ATTACHMENT
POINTS

SEUTS
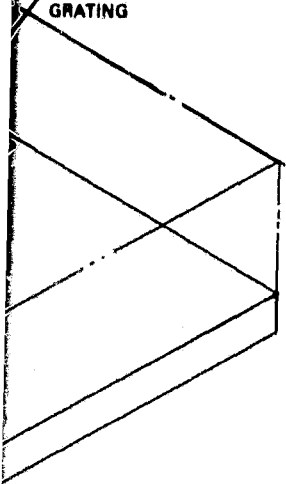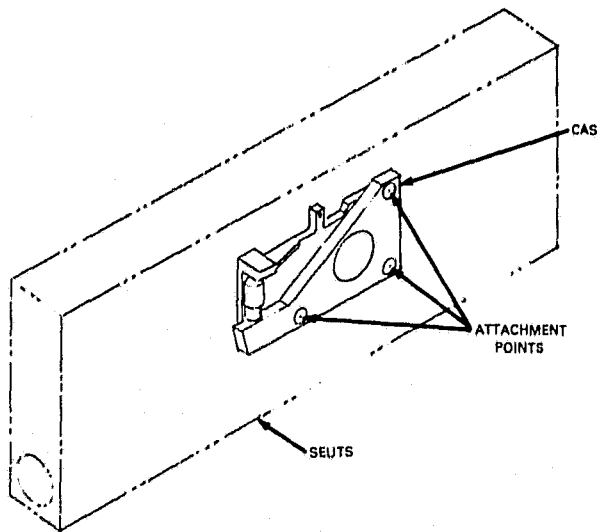
OPTIONAL CAS ATTACHMENT

record the entire spectral range with the least compromise to the high spatial and spectral resolution offered by the instrument. Recognizing that short-lived but rarely occurring solar phenomena can best be studied with sensitive photoelectric detectors not limited by film footage, we also will perform an engineering evaluation of such a detector on the first flight. More detailed descriptions of the various subsystems are presented in the following sections and a summary of performance characteristics is provided in Section III.E.

2. Extreme Ultraviolet Telescope

A Wolter Type II grazing-incidence telescope [8] with an effective focal length of 4.24 m is used to provide an image of the sun in EUV and visible light to the entrance slit of the spectrograph. Angles of incidence of 10°-13° are used to achieve high (60%) reflectivity at 22.5-37.0 nm. Two optical elements --a paraboloidal primary followed by a hyperboloidal secondary produce a usable FOV of 8 arcmin within which the theoretical resolution is < 1/4 arcsec on a curved focal plane. (A flat spectrograph entrance aperture can be located to achieve 2 arcsec or better within a 4 arcmin field.) At F/22, the telescope matches the high-resolution toroidal-grating design and has 47% of the total aperture that an unobscured F/22 telescope would have.

A half-sized telescope has been designed, built, evaluated and space qualified. All parts are made of zero-expansion Cervit and are bonded with a specially-selected adhesive to avoid thermal distortions. The existing unit can resolve slits separated by 3 arcsec (center-to-center) distinctly at visible wavelength and usably at 30.4 nm. It has been verified by ray-tracing that spatial resolution of the twice larger unit would be improved by a factor of 2, i.e. about 1.5 arcsec, even if absolute linear surface deviations and linear misalignments are no better than the current telescope. We are confident that experience gained on the first unit and the use of more sophisticated polishing techniques will provide a resolution of 1-1.5 arcsec with the new telescope.

3. Entrance Slit and Shutter

A commandable mechanism, based on the design used in the UV spectrometer and polarimeter (UVSP) to be flown on the Solar Maximum Mission, will permit selection of one of four entrance apertures (described in Section III.B.). The UVSP unit has achieved uniformity of slit dimensions to within 1μm, 10% of our narrowest aperture width. It positions each slit on the nominal optical axis to within 8μm, which in our design corresponds to 0.4 arcsec at the telescope focal surface. An aluminum filter will be attached to each aperture (except, perhaps, the narrowest) to prevent radiation to the red of 70 nm from entering the spectrograph, thus eliminating the major source of scattered light. The optically polished front face of the aperture plate is tilted 7.5° from the telescope's optical axis, presenting a solar image with the entrance aperture superposed to the H-α slit jaw camera (see Section III.C.9.).

The entrance shutter will be a plate mounted on a stepping motor shaft. The time increment from full closed to full open (and the reverse) will be $\lesssim$ 20 msec, much shorter than the shortest expected exposure time.

4. Toroidal Grating

A grating ruled on a toroidal surface provides stigmatic imaging at up to two wavelengths and quasi-stigmatic imaging over an extended wavelength range if operated at near-normal incidence[9]. Thus the relatively poor XUV reflectivity of the grating at normal incidence is more than compensated by the fact that spatial information along the spectrometer's entrance slit is preserved. The nominal grating parameters for our proposed design represent a compromise among numerous criteria, such as minimization of aberrations over the full wavelength range, matching of spot sizes to detector resolution, maximization of radiation density in the focal plane, and satisfying rather conservative constraints imposed on the optical layout by structural considerations (Figure 2a). The image detector will be placed at the concavely curved tangential focus of the toroidal grating to obtain best spectral resolution at all wavelengths.

Extensive ray-tracing calculations have verified this design and established its off-axis performance as well as its sensitivity to misalignment and defocusing effects. These calculations show that the proposed grating design can theoretically provide an on-axis image less than 5 μm in diameter at the stigmatic wavelengths. Folding these results for the classically ruled grating with nominal values for the other optical elements in the system (see Figure 2b and c) indicates that the detected spatial and spectral resolutions will be no worse than 2 arcsec and .0055 nm respectively, over a full 4-arcmin field of view on the sun and over the entire wavelength range of 25.0 to 37.0 nm. Along the Rowland plane, the spectral resolution will be .0044 nm at all wavelengths and the spatial resolution will be 1.3 arcsec at the stigmatic points. This is sufficient for measurements of line profiles even under quiet sun conditions. These values will be improved if detailed structural studies show that the layout constraints mentioned above can be relaxed. They would also be somewhat improved if the toroidal grating were holographically ruled which permits a greater degree of aberration correction than is possible with a classically ruled grating.[10]

5. EUV Roll-Film Camera

The optical system described presents a focal "plane" with ~ 700,000 spectral-spatial resolution elements to be recorded simultaneously, pointing to film for the prime data taking mode. Because of the small size of each element (≲ 20μm square) and the need for high speed, Eastman Kodak 101-07 film will be used. With a quantum efficiency of ~ 3%, it is the most sensitive photographic film for our wavelength region. However, this film does have certain handling difficulties[11]; for example, the surface is so susceptible to abrasion that each edge is coated with a raised strip of polystyrene beads to prevent adjacent convolutions of a roll from touching each other.

Figure 2d includes a concept drawing of the roll-film camera being developed for SEUTS. The design has been kept simple to maximize mechanical reliability, and camera materials and coatings selected to prevent fogging of the film by contact with them or by spark discharges.[12] The design, based on space-qualified motors and servos, has been extensively analyzed as discussed in Appendix AIII. The film transport is servocontrolled to maintain a low, constant film tension (~ 0.5 lb.) regardless of the amount of film on each spool. Power is applied to the film advance system only during film motion (~ 16 watts for ~ 1 s) and to the film hold-down system (see Appendix) only when its state is changed (12 watts for ≲ 1 s).

"TYPICAL" DETECTED RESOLUTIONS VS. SYSTEM DESIGN

DETECTOR RESOL. = 0μm   **DETECTOR RESOL. = 10μm**   **DETECTOR RESOL. = 25μm**

SPECTRAL RESOLUTION (nm) vs SPECTROGRAPH MAGNIFICATION

SPATIAL RESOLUTION (arcsec) vs SPECTROGRAPH MAGNIFICATION
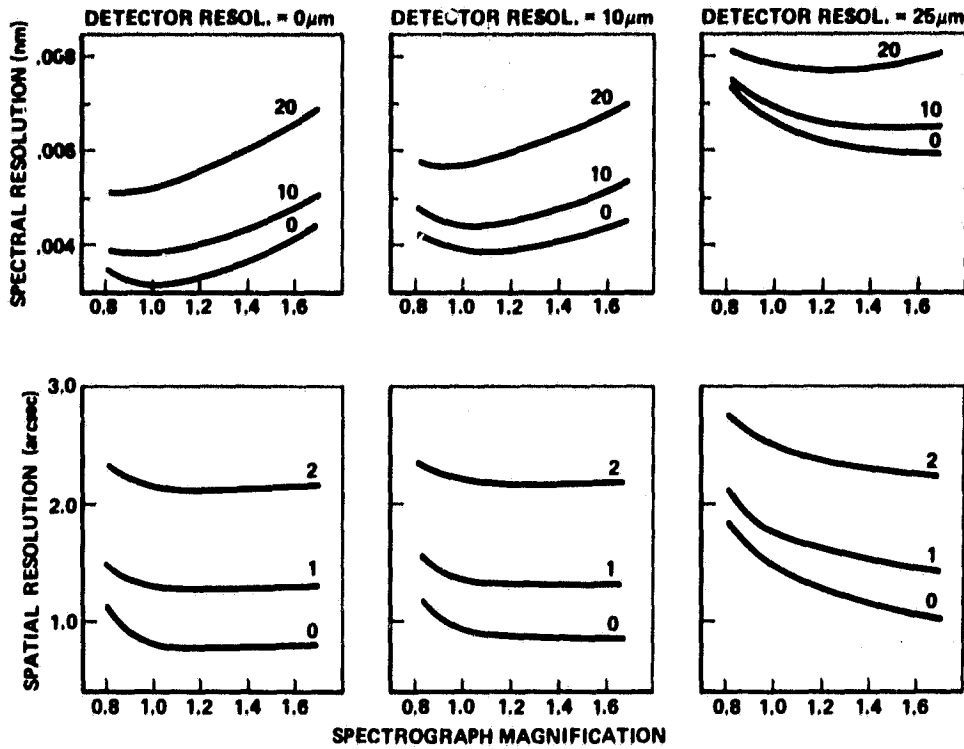
Fig. 2a. "Typical" system resolutions as a function of spectrograph magnification, including grating aberrations and surface errors. Spectral resolution curves are given for entrance slits of 0, 10, and 20μm ; spatial curves for telescope spot sizes of 0, 1, and 2 arcsec.

DETECTED RESOLUTIONS VS. WAVELENGTH AND DISTANCE OFF ROWLAND PLANE

(a) ON ROWLAND PLANE
(b) ±2 arcmin OFF PLANE
(c) ±4 arcmin OFF PLANE

SPATIAL RES. (arcsec) vs WAVELENGTH (nm)

SPECTRAL RES. (nm) vs WAVELENGTH (nm)
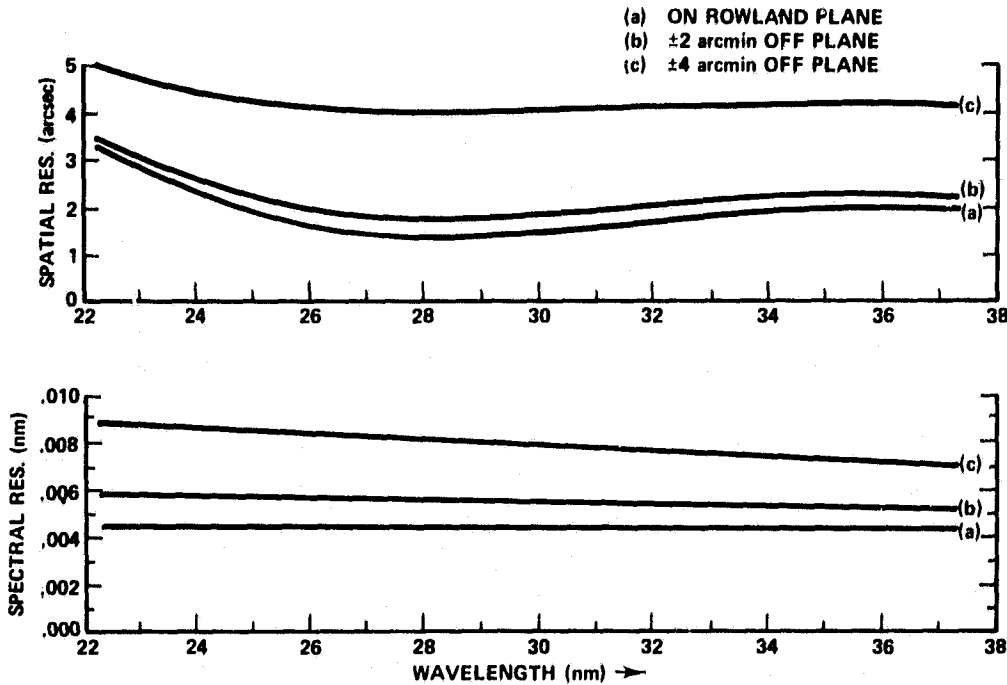
Fig. 2b. System resolutions versus wavelength for the nominal design, including grating aberrations and surface errors for a mechanically ruled toroid. These ray-trace calculations assume a 10μm entrance slit, 1 arcsec telescope performance, and 10μm detector resolution; off-plane curves include effects of telescope defocus.

IN
ROWLAND
PLANE

2 arcmin
OFF
ROWLAND
PLANE

28.4n

Fig. 2c. Ray-trace spot diagrams proposed design, including grating for all calculations shown in Fig the mechanically ruled grating to

INVERTED "HAT" RING
AND SCREEN MESH
PHOTOCATHODE

BIAS RING
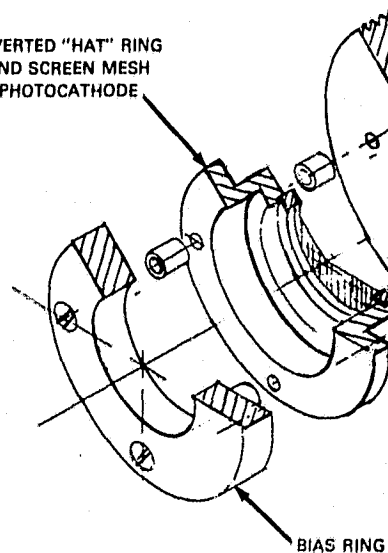
Fig. 2e. Amplify

TOROIDAL GRATING SPOT DIAGRAMS

10μm

10μm   .002nm

1 arcsec

28.4nm   33.5nm
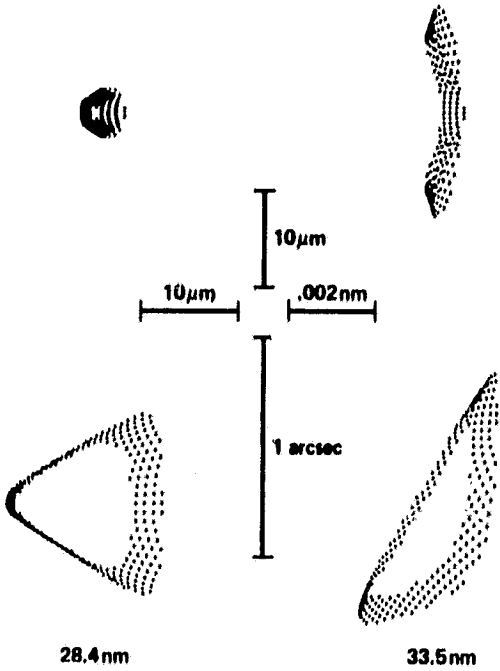
spot diagrams at 28.4 and 33.5nm for the nominal
cluding grating aberrations only. The focal plane
s shown in Fig. 2 is set at the tangential focus of
led grating to provide optimum spectral resolution.
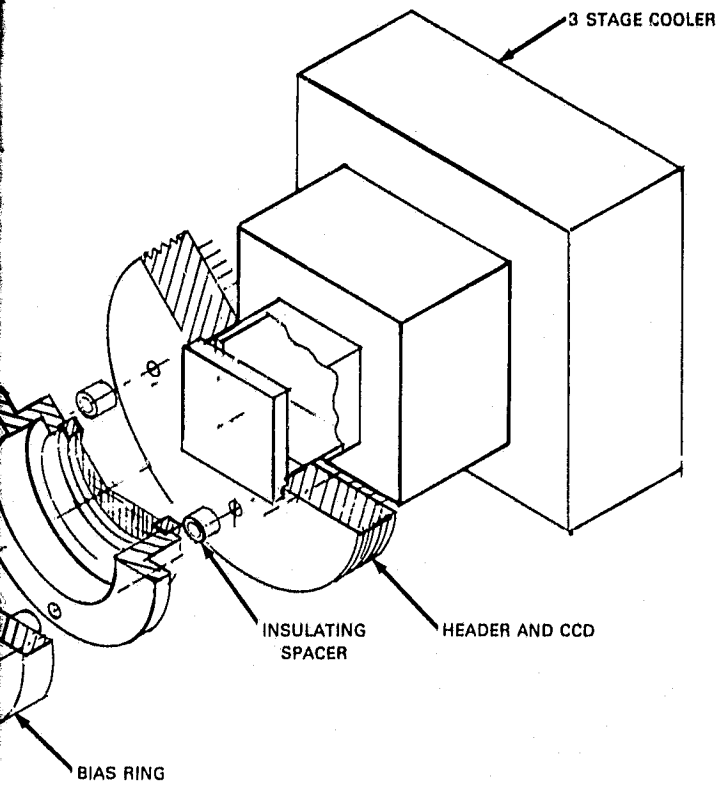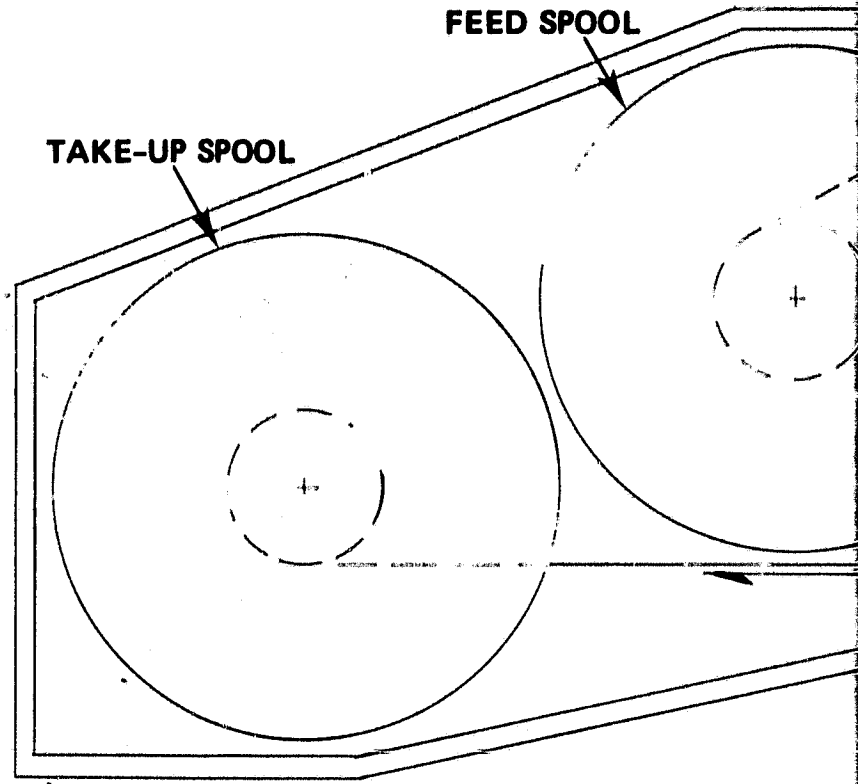
3 STAGE COOLER

INSULATING
SPACER

HEADER AND CCD

BIAS RING

2e. Amplifying Image Detector (AID)

FEED SPOOL

TAKE-UP SPOOL

D.C.
TORQUE MOTOR-
TACHOMETER

ELECTRONIC BRAKE

Fig. 2d.   EUV Roll Film Ca

FOLDOUT FRAME 2

DANCER

FILM PLATEN
(defines focal plane)

FEED SPOOL

TAKE-UP SPOOL

CAMERA
DOOR

HOLD-DOWN
MASK

IDLER
PAIR

DANCER
(idler pulley on
spring loaded arm)

D.C.
TORQUE MOTOR-
TACHOMETER

ELECTRONIC BRAKE
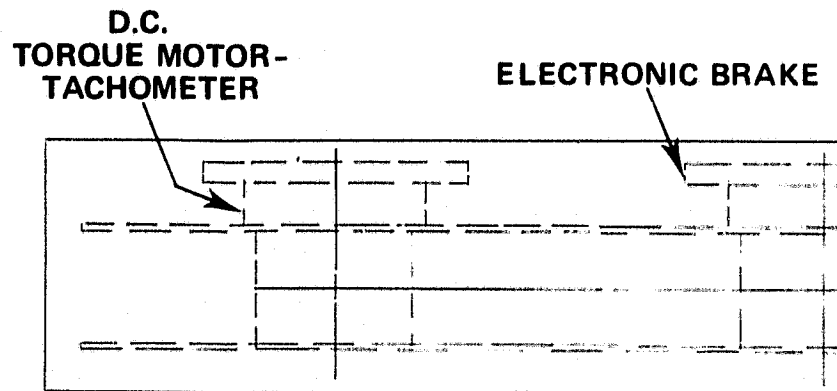
Fig. 2d.   EUV Roll Film Camera

The modular camera body acts as a film vault, maintaining a benign environment for the film before, during, and after the mission. The unit can be accurately and easily installed into the spectrograph during the last stages of Shuttle integration. Its capacity (up to 600 ft. of film can be accommodated in the present design) will permit almost 2300 exposures at the dispersion of 0.21 nm/mm. Estimating conservatively, 200 exposures will be used for spectral diagnostics of various coronal features, 800 to record evolutionary aspects of active regions, bright points and coronal holes, and 500 held in reserve for flare studies on targets of opportunity.

6. Calibration, Annotation and Alignment

Data reduction of photographic spectra requires knowledge of three properties: (a) Relative intensity as a function of film density (H&D curve) in the radiation of interest; (b) Relative efficiency of the entire system as a function of wavelength; and (c) Absolute intensity calibration of at least one line. The NRL Skylab experience shows that the H&D characteristic must be obtained from the flight films themselves,[11] in the radiation of interest. Therefore, we will construct H&D curves from quiet sun spectra taken with different exposure times. Sets of spectral lines with well known theoretically calculated intensity ratios will be used to establish (b). The efficiency curve can be updated if it changes with time. From the NRL Skylab data reduction, we believe that relative line intensities accurate to better than ± 20% can be obtained.[13,14]

The absolute intensity of at least one line in the exposed range must be known to put the entire set of measurements on an absolute scale. At present, the absolute intensities of several lines from 22.5 nm to 37.0 nm have been measured at least once for the quiet sun.[15] We believe that such data will be sufficient, but if we find that a better absolute scale is needed, we will make use of the EUV calibration facility at the NBS synchrotron (SURF).

Recording the exact times of start and finish of each exposure, slit configuration, and pointing and roll information will be vital, especially when ~ 2000 exposures are taken over the course of several days. Such information will be telemetered to the ground via the instrument microprocesser in conjunction with the exposure number which will be encoded on the film by means of a blue-green LED array flasher.
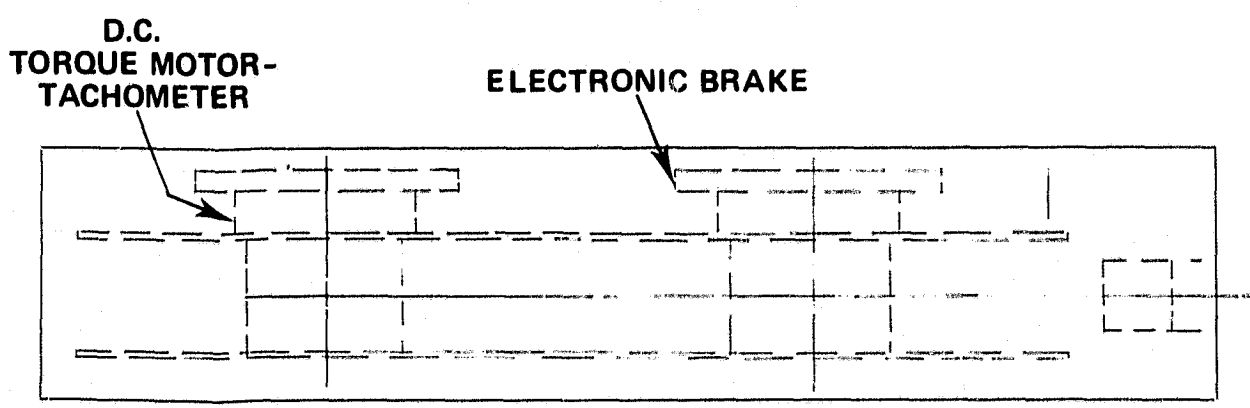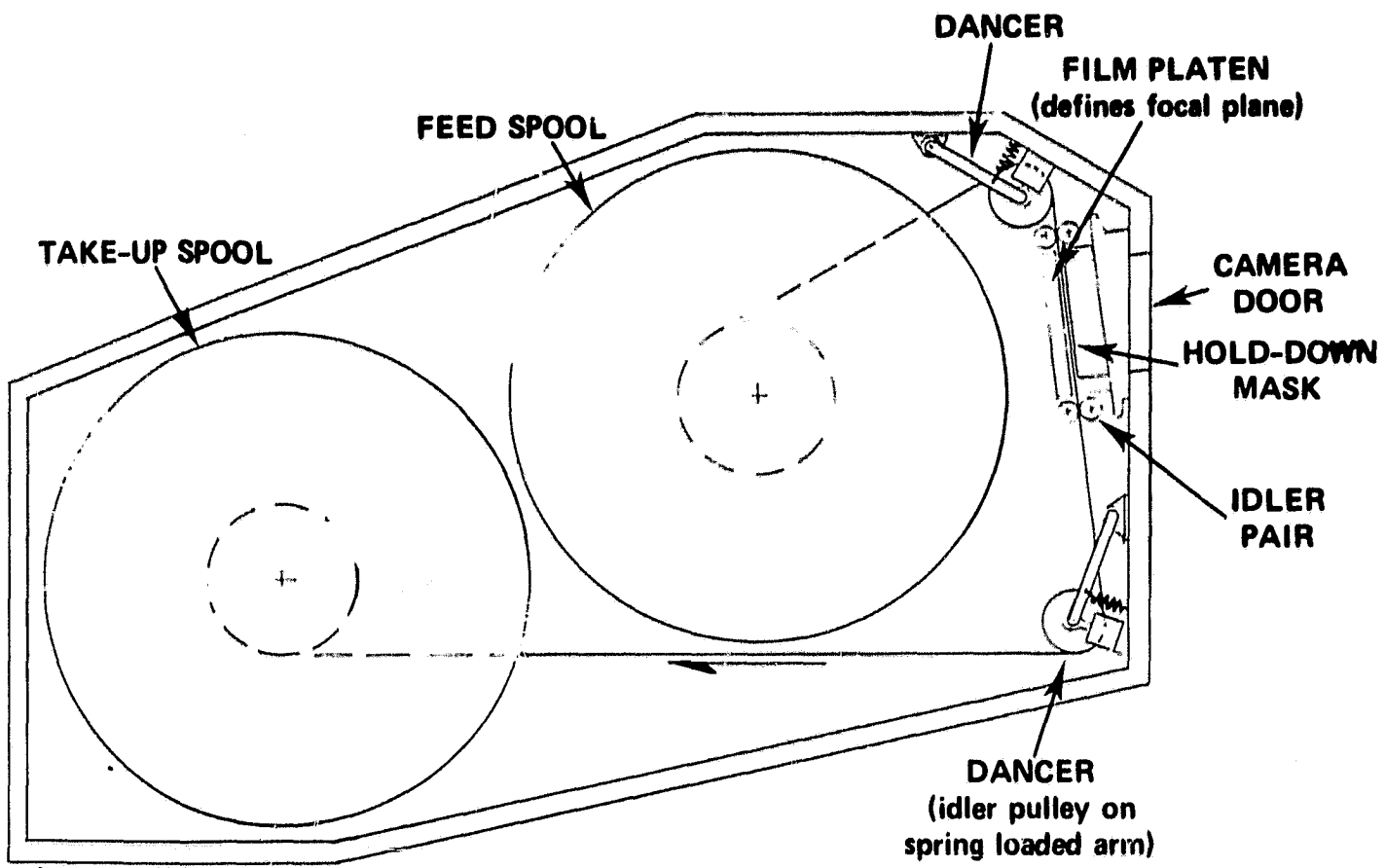
In order to check that the EUV zero-order monitor (exposure meter) is operating properly during the flight we will mount a very weak radioactive source, possibly Fe 55, in front of the sensor and confirm that the observed source count rate is nominally the same as it was during preflight calibration. The source will produce a rate of 2-5 counts per second, which is 10 times the MEM detector's background count rate.

Initial alignment of the telescope-spectrograph system, as well as pre- and post flight verification of that alignment, will be done in air at visible (546.1 nm) wavelengths. A "focus grating" of 200 l/mm groove density ruled on either side of the 3600 l/mm EUV rulings will be used for this work. Final alignment and the instrumental profile will be measured both before and after the flight using an XUV narrow-line source such as a water-cooled sliding spark with yttrium electrodes.[16]

7.   Instrumental Sensitivity

Expected SEUTS exposure times in the photographic mode can be estimated directly
from the nominal properties of its optical systems and known solar radiances
in the emission lines of interest. Such radiance measurements were made by
OSO-7 but only over a 12 x 20 arcsec pixel size. Their use provides only
upper limits to exposure times for structures such as loops that are known to
be more compact than this in at least one dimension.

The expected photon density integrated over a spectral line, at the final film
plane, is given by

$$R \cdot A_T \cdot \Omega_{pixel} \cdot R_T \cdot R_G \cdot T_{filter} \cdot A_i^{-1}$$

where R is the solar radiance at λ; A_T is the area of the telescope aperture;
Ω_{pixel} is the solid angle of the pixel (determined by actual slit width and
nominal slit length corresponding to a 2 arcsec spatial resolution); R_T is the
reflectance of the telescope; R_G is the reflectance of the grating; T_{filter}
is the transmission of the visible light blocking filter; and A_i is the area
illuminated on the film by one pixel. Two extreme solar features are considered,
one an active region reported to be "near flare brightness" in Hα, the other
a coronal hole (but not the deepest that could be found during the OSO-7 mission).
For each feature, two modes of operation are analyzed - a wide slit or spec-
troheliograph mode with the final pixel size determined primarily by telescope
resolution (2 arcsec) and a narrow slit or line profile mode with the final
pixel size in the direction of dispersion determined by slit size and grating
aberrations. Table III-1 summarizes nominal SEUTS characteristics and
Table III-2 provides estimates of photon densities and exposure times. A film
sensitivity of 2.0 x 10^{8} ph cm^{-2} for a film density of 0.2 on Eastman Kodak 101
film has been used, based on interpolation of measurements at $\lambda \leq 4.4$ nm[17]
and data at $\lambda \geq 73.5$ nm.[18]

8.   Amplifying Image Detector (AID)

Although film is unmatched in storage capability and resolution, it does have
severe limitations: Its sensitivity, although less than that of photoelectric
devices, necessitates very careful handling. Its dynamic range is small com-
pared to solar intensity variations, requiring multiple exposures which, to-
gether with film transport time, limits temporal resolution. Its bulk, and
the difficulty of changing film magazines on orbit, restricts the strategy
of initiating a flare mode while observing a likely site before a flare begins.

We, therefore, include a photoelectric AID placed to observe wavelengths from
33.5 to 35.7 nm. This wavelength band, in the region of greatest instrumental
throughput, includes several density and temperature sensitive coronal and
flare lines. Among designs for the AID that we have evaluated,[20] our first
choice is a semitransparent electroformed mesh coated with a photoemissive
material[21] (e.g., Mg F$_2$) used with a proximity-focused backside thinned CCD
array (Figure 2e.

Calculations (Appendix AIV) indicate that the device should detect single
photoelectrons if the CCD is cooled. The dynamic range per pixel per exposure
will be 550-730, dictated by CCD well capacity and the accelerating voltage.

TABLE III-1 SEUTS CHARACTERISTICS

λ	A_{Tel} cm^2	R_T(1)	R_G(2)	T_{Filter}(2)	T_{Filter}(3)
33.5nm	140	.34	.024	.325	.57
30.4nm	140	.34	.019	.35	.59
28.4nm	140	.33	.014	.37	.61
27.0nm	140	.33	.0115	.38	.62
26.4nm	140	.32	.01	.39	.62
24.1nm	140	.32	.005	.42	.65

(1) Based on data published in Reference 19.

(2) As reported for the NRL S082A instrument[7] and to be used in wide-field mode only.

(3) Half-thickness filter to be used in narrow slit (10μm) mode.

TABLE III-2. Typical SEUTS Focal Plane Photon Densities (ρ) and Exposure Times (T)

Coronal Active Region

λ (nm)	R(1)	Wide-Field(2) Mode		Line Profile Mode(3)	
		ρ(4)	T(5)	ρ	T
33.5	3x10^4	8.6x10^8	.23	7.6x10^8	.26
30.4	7.2x10^4	1.6x10^9	.13	13.5x10^8	.15
28.4	1.7x10^4	2.7x10^8	.74	2.2x10^8	.90
27.0	.81x10^3	1.0x10^7	20	0.8x10^7	24
26.4	1.6x10^3	1.8x10^7	11	1.4x10^7	14
24.1	1.7x10^2	9x10^5	210	7.0x10^5	290

Coronal Hole

R	Wide-Field Mode(2)		Line Profile Mode(3)	
	ρ	T	ρ	T(6)
108	3.1x10^6	65	2.7x10^6	74
7000	1.6x10^8	1.2	1.3x10^8	1.5
97	1.5x10^6	130	1.2x10^6	160
19	2.4x10^5	830	2.0x10^5	1000
38	4.0x10^5	500	3.2x10^5	620
45	2.3x10^5	870	1.8x10^5	1100

(1) units of erg cm^{-2} s^{-1} sr^{-1}

(2) assumes a 2x2 arcsec pixel size (45x45μm)

(3) assumes a 20x45μm pixel size

(4) units of photons cm^{-2} s^{-1}

(5) units of seconds

(6) Exposures of up to 1200 s were found to be feasible for high resolution spectrographs on ATM.

At the expense of temporal resolution, this can be extended and weak line statistics improved by co-adding frames during analysis. The center-to-center spacing (23μm) of the CCD pixels will limit the spatial resolution to ≈ 20 lp/mm.

Because of the windowless construction of the AID, a high vacuum (better than 10^{-5} torr) must obtain throughout the spectrograph. High voltage will, therefore, not be applied to the AID for the first few days of the mission. A flat, gold-coated mirror will be rotated into position at grazing incidence to direct EUV radiation onto the AID (Figure 1). To avoid interference with photographic observations, the AID will be deactivated whenever the film camera is open and, indeed, may not be used until the last few days of the mission.

On the first flight we will use the AID to assess the problems of operating a windowless detector in the Orbiter/Spacelab environment, assess whether its predicted operating characteristics can be maintained over the long prelaunch integration period and make an initial search for rapidly time-varying phenomena. Depending on results obtained, one or more of these sensors may be located in the principal focal plane on subsequent missions to pursue further studies of rapidly time-varying phenomena.

9.   Hα Slit-Jaw Monitor

The instrument incorporates a slit-jaw monitor that produces an image of the EUV spectrograph-slit superimposed on an image of the solar chromosphere as seen in Hα at 656.3 nm. This will provide a direct operational means of aiming the SEUTS at solar features which have distinctive Hα signatures. We will also use the monitor to calibrate the SEUTS pointing control, allowing us to target other features by means of their absolute (or relative) coordinates. During data analysis, the slit-jaw images will assure unambious registration of the EUV data with observations, such as magnetograms, made from the ground or from co-flying Spacelab instruments.

The polished faces of the entrance-slit assembly reflect into the Hα monitor an 8 x 5 arcmin portion of the solar image produced by the telescope in which the image of the slit itself appears darkened. The optics consist of a train of three refocusing lenses, two solid Fabry-Perot etalons, a blocking filter, and infra-red (heat) absorbing glass. The Fabry-Perot interference filters are temperature controlled to keep wavelength drifts below ± .013 nm. Two filters are used in tandem to suppress continuum transmission and thus increase the contrast of the detected image. The pair of fused silica etalons transmit ~ 20% of the incident flux within a passband of .07 nm FWHM.

The Hα image is recorded by a CCD detector which provides a spatial resolution of 3 to 4 arcsec with good signal to noise in an integration time as short as 0.1 s. For adequate coverage of transient phenomena, the Hα image will be read out every 10 s whenever EUV observations are being made. Much of the read-out electronics will be common to the EUV AID readout (described in Section III.C.8) for reduced cost (see Appendix AV.).

D.   SEUTS System Design

1.   Mechanical Design

To meet the requirement of a rigid, stable optical bench we use an "egg-crate" of aluminum-alloy face sheets that form a sandwich with a core of aluminum-alloy

webbing (Figure 1). The assembly is joined by a hot, dip-brazing technique; mounting pads and "heat-pipe" conduits running lengthwise are designed into the plate <u>before</u> the brazing process. Other methods (solid plate, ribbed, or isogrid solid plate) could be used; however, the "egg-crate" design provides dimensional stability, minimum weight, and is less expensive to manufacture. Such an "egg-crate" design is being successfully employed on the Solar Maximum Mission (SMM) program.

The designs for both the instrument door and spectrograph entrance aperture mechanisms are based on designs used on the SMM program; only minor modifications are required. The SEUTS can be mounted to the Instrument Pointing System (IPS) or to an offset pointer (e.g. CAS) with a three point kinematic mount (Figure 1).

2.   Thermal Design

The SEUTS will be aligned and operated at room temperature. Preliminary results of a complete thermal analysis of the proposed design indicate that it is relatively insensitive to bending and side-to-side distortions. However, since its focus is sensitive to longitudinal displacements, the structure must be held at $20 \pm 4^{\circ}C$ and heat pipes will be used to minimize temperature differentials from front to rear of the instrument ($\Delta T \lesssim 1^{\circ}C$ can be achieved by this means). Passive thermal control will be used wherever possible with heaters used as necessary to maintain the minimum operating temperature. Use of an external thermal canister with variable heat pipes would be highly desirable to minimize the possibility of film damage due to excessive heat upon Shuttle re-entry. It would also minimize the thermal design required to counteract the adverse orbiter environment.

3.   Instrument Control Philosophy

The SEUTS will be controlled by a instrument dedicated microprocessor for which a preliminary design has been developed[22] (see Appendix AVI.). Command sequences needed to carry out observing programs will be stored in the microprocessor, with each command tagged by a relative time. When a sequence is initiated, from the POCC or AFD, the microprocessor will keep track of elapsed time and will execute individual commands at the proper moment. The microprocessor will be interruptible, so that real time commands can be sent to the instrument or a flare mode initiated by an on-board monitor. Stored timelines may be updated while the microprocessor is executing command sequences.

E.   Instrument Performance Summary

The overall instrumenal performance is summarized below. Resolution values were determined by ray-tracing calculations and include broadening due to telescope imperfections, off-axis defocusing, a 10μm entrance slit, grating aberrations, grating surface errors, and the film grain size. We assume that the grating is mechanically ruled and the feeding telescope has 1 arcsecond performance on axis. "Best" values are at the stigmatic wavelengths and/or in the Rowland plane; "typical" values represent an average over the field of view and wavelength range.

Wavelength range:	22.5 - 37.0 nm
Field of view:	8 arcmin x 0.5 arcsec in line profile mode
	8 arcmin x 5 arcmin in wide field mode
Number of exposures:	~ 2000
Spatial resolution:	1.3 arcsec (best); 2.0 (typical)
Spectral resolution:	.0044 nm (best); .0055 (typical)
Temporal resolution:	3 s (best); 60 (typical)
Telescope Aperture:	140 cm^2

F.   SEUTS Pointing Requirements

An analysis of stabilization requirements and other pointing operations for
SEUTS are contained in Appendix VII.

G.   Uncertainties and Obstacles

Most of the uncertainties in this proposal concern the interfaces to Spacelab.
The final thermal design cannot be scoped until the Shuttle environment is known.
We have assumed that our internal thermal design will be used to minimize tem-
perature gradients but that a controlled shroud (as e.g. the OFT-4 thermal
canister) will be available to provide a benign external environment. A versatile
pointing interface, i.e. a system of co-alignment of instruments on IPS or an
independent pointer, is needed to optimize science. Several options are com-
patible with our instrument but no costs have been included. Reflight costs
are dependent on extent of changes of interfaces for which no guidelines have
been given. Only a nominal reflight cost can be provided.

H.   Supporting Studies and Desired Concurrent Observations

We will encourage and maintain contact with efforts to develop coronal heating
theories, models of flare trigger mechanisms etc. in order to assure that our
instrument provide meaningful tests of these theories. However, no supporting
studies are specifically required under this proposal.

A correlation of intensity fluctuations in the EUV with spectral velocity data
in the visible region of the spectrum from the Solar Optical Universal Polari-
meter will enable one to estimate the spatial-phase relationship in height for
atmospheric oscillations. In so doing, estimates concerning the penetration
and attenuation of vertically propagating oscillations could possibly discern
the levels at which mechanical energy is dissipated. This has important impli-
cations concerning the nature of temperature and ionization structure of the
transition zone and upper chromosphere, and the means by which the solar atmo-
sphere maintains thermal equilibrium.

Additionally, oscillations present in the periphery of sunspots, so-called
running penumbral waves as observed in H-alpha, could possibly be detected in
He II 30.4 nm. Detection of intensity fluctuations above sunspots with periods
comparable to that observed in H-alpha would suggest the dissipation of mechanical
energy from Alfven or fast-mode coupled waves. Such observations would have
direct impact on models involving sunspot energy balance, and would suggest
that the continuum energy deficit associated with the presence of a spot is
balanced by magnetically coupled wave dissipation at EUV forming levels of the
solar atmosphere.

Recent rocket observations by the High Resolution Telescope and Spectrograph (HRTS)
reveal what seem to be minute high velocity jets of material in the solar tran-
sition zone which persist for at least several minutes.[22] Simultaneous measure-
ments by SEUTS and HRTS would test the suggestion that these jets represent a
major source of coronal heating by directly recording their influence on the
overlying coronal layers and by determining whether or not they have any high-
temperature counterparts.

Co-flying instruments which are especially sensitive to the earliest phases of
solar flares, such as an X-ray telescope, could be used to provide a flare alarm

signal to SEUTS that would initiate preloaded high-rate observing sequences,
as mentioned in Section III.D.3. The concurrent flare observations by these
other instruments would also be of great value during data analysis.

IV. DATA REDUCTION AND ANALYSIS

A. Film Data Reduction

Upon retrieval, the film will be stored under controlled conditions. Prior to
development it will be cut into 30 ft. segments and then processed in accordance
with practices developed during the Skylab mission. The developed strips will
be divided into one or two frame segments and mounted between high quality glass
plates. Storage will be in a controlled environment. Together with film cali-
bration and annotation, this will be the format in which the data are supplied
to the National Space Science Data Center under the schedule specified.

Portions of selected frames--time sequences, etc--will be selected for digiti-
zation and quantitative analysis. A suitable microdensitomer is available from
the Landsat program although it must be supplemented by appropriate tape drives.
Standard software already exists for an existing minicomputer to carry out
routine processing on the digitized images. Software that would need to be pro-
duced for SEUTS is that necessary to derive physical parameters of the emitting
plasma, such as line of sight emission measures, densities from line ratios, and
line widths (profiles) as a function of spatial location. In addition, absolute
wavelengths will be obtained for the purpose of line identification and Doppler
shift analysis. A Grant comparator with computer compatible output is available
in the laboratory.

B. Photoelectric Data Reduction

Both Hα and photoelectric (AID) data will be displayed on the GSE in analog form.
Further, it will be stored in digital form for subsequent analysis on the existing
minicomputer. Except, possibly, for reformatting on a main frame computer, all
additional processing will be identical to that required for the digitized film.

C. Data Analysis and Interpretation

The modeling calculations needed to support interpretation of the SEUTS data
will be carried out at the computing center of the Sciences Directorate at Goddard.

V. RESULTS TO BE OBTAINED

Line-of-sight emission line intensities over a wide range of transition region
and coronal temperatures for many types of features (active regions, quiet sun,
coronal holes, etc.) as a function of their spatial coordinates--Emission line
profiles and possible Doppler shifts of coronal plasmas, correlated with condi-
tions of electron temperature and density in which they are found--Intensity
variations of spectral lines as a function of time, spatial coordinates and tem-
perature for evolving regions and transient phenomena--Inferred coronal and tran-
sition region magnetic field configurations, their correlation with density and
temperature as a function of height and changes with active region evolution and
flare activity--Spatial and temporal distribution of flare plasmas with densities
inferred from emission line ratios.

These observations will be used to evaluate and improve models of the solar
corona and the processes of energy and mass transport, magnetic field propagation
and particle acceleration that take place there.

AI. Examples of Diagnostic Emission Lines (with Fractional Changes of Intensity per Decade Change in Density) Available in the 22.5 - 37 nm Spectral Band

		$\log_{10} N_e$			
		9.5	10.5	11.5	12.5

He II T_e 6×10^4 K

$1s^2\ ^1S_0 - 1s2p\ ^1P_1$	303.78				
$^1S_0 - 3p\ ^1P_1$	256.317				
$^1S_0 - 4p\ ^1P_1$	243.027				
Limit	227.84				

C IV T_e 1×10^5 K

$2s\ ^2S_{1/2} - 2p\ ^2P_{1/2}$	312.453				
$^2S_{1/2} - {}^2P_{3/2}$	312.422				

N IV T_e 1.3×10^5 K

$2s^2\ ^1S_0 - 2s3p\ ^1P_1$	247.205				

O IV T_e 1.4×10^5 K

$2s^3 2p\ ^2P_{3/2} - 2s^2 3s\ ^2S_{1/2}$	279.933				
$^2P_{1/2} - {}^2S_{1/2}$	279.631				
$^2P_{3/2} - 2s^2 3d\ ^2D_{3/2}$	238.571				
$^2P_{1/2} - {}^2D_{3/2}$	238.360				

O V T_e 2.2×10^5 K

$2s2p\ ^1P_1 - 2s3s\ ^1S_0$	248.459				

Mg VI T_e 5×10^5 K

$2s^2\ ^2P^3\ ^2P_{3/2} - 2s2p^4\ ^2S_{1/2}$	314.658	2.8	1.3	1.0	1.0
$^2D_{3/2} - {}^2P_{1/2}$	268.986	1.3	1.1	1.0	1.0

Mg VII T_e $6. \ 10^5$ K

$2s^2\ 2p^2\ ^3P_1 - 2s2p^3\ ^3P_2$	365.222	0.8	0.9	1.0	1.0
$^3P_0 - {}^3P_1$	363.770	0.9	0.9	1.0	1.0
$^1S_0 - {}^1P_1$	320.490	3.0	1.4	1.0	1.0
$^1D_2 - {}^1P_1$	280.744	3.0	1.4	1.0	1.0

Fe IX T_e 9×10^5 K

$3p^6\ ^1S_0 - 3p^5 3d\ ^3P_1$	244.909	0.9	0.8	0.9	1.0
$^1S_0 - {}^3P_2$	241.739	0.7	0.2	0.1	0.1

Si IX T_e $1.0 \ 10^6$ K

$2s^2 2p^2\ ^3P_2 - 2s2p^3\ ^3D_3$	349.87	1.0	0.8	0.9	1.0
$^3P_0 - {}^3D_1$	341.96	0.8	0.8	0.9	1.0
$^1D_2 - {}^1D_2$	258.08	4.3	2.5	1.3	1.0

Mg IX $\qquad$ T_e $\quad$ 1. $\times 10^6$ K

$\qquad$ $2s^2\ ^1S_0 - 2s2p\ ^1P_1$ $\qquad$ 368.071 $\quad$ 1.0 $\quad$ 1.0 $\quad$ 1.0 $\quad$ 1.0

Fe X $\qquad$ T_e $\quad$ 1.3 $\times 10^6$ K

$\qquad$ $3s^2\ 3p^5\ ^2P_{3/2} - 3s3p^6\ ^2S_{1/2}$ $\quad$ 345.746 $\quad$ 1.0 $\quad$ 1.0 $\quad$ 1.0 $\quad$ 1.0

Fe XI $\qquad$ T_e $\quad$ 1.4 $\times 10^6$

$\qquad$ $3s^2\ 3p^4\ \begin{array}{l}^1D_2 \\ ^3P_2\end{array} - 3s3p^5\ \begin{array}{l}^1P_1 \\ ^3P_1\end{array}$ $\quad$
308.607 $\quad$ 2.4 $\quad$ 2.0 $\quad$ 1.2 $\quad$ 1.0
341.146 $\quad$ 1.0 $\quad$ 0.9 $\quad$ 0.9 $\quad$ 1.0

Si X $\qquad$ T_e $\quad$ 1.5 $\times 10^6$ K

$\qquad$ $2s^2 2p\ \begin{array}{l}^2P_{3/2} \\ ^2P_{1/2}\end{array} - 2s2p^2\ \begin{array}{l}^2D_{5/2} \\ ^2D_{3/2}\end{array}$ $\quad$
356.01 $\quad$ 1.3 $\quad$ 1.0 $\quad$ 1.0 $\quad$ 1.0
347.39 $\quad$ 0.8 $\quad$ 0.9 $\quad$ 1.0 $\quad$ 1.0

Fe XII $\qquad$ T_e $\quad$ 1.6 $\times 10^6$ K

$\qquad$ $3s^2\ 3p^3\ \begin{array}{l}^2D_{5/2} \\ ^4S_{3/2} \\ ^4S_{3/2}\end{array} - 3s3p^4\ \begin{array}{l}^2D_{5/2} \\ ^4P_{1/2} \\ ^4P_{3/2}\end{array}$ $\quad$
338.270 $\quad$ 1.8 $\quad$ 1.3 $\quad$ 1.1 $\quad$ 1.0
346.810 $\quad$ 0.7 $\quad$ 0.6 $\quad$ 0.7 $\quad$ 0.9
352.130 $\quad$ 0.7 $\quad$ 0.7 $\quad$ 0.7 $\quad$ 0.9

S XI $\qquad$ T_e $\quad$ 1.6 $\times 10^6$ K

$\qquad$ $2s^2 2p^2\ \begin{array}{l}^3P \\ ^3P_1 \\ ^3P_1\end{array} - 2s2p^3\ \begin{array}{l}^3D_3 \\ ^3D_2 \\ ^3D_1\end{array}$ $\quad$
291.59 $\quad$ 2.0 $\quad$ 1.0 $\quad$ 0.9 $\quad$ 0.9
285.83 $\quad$ 1.1 $\quad$ 0.9 $\quad$ 0.8 $\quad$ 0.9
281.40 $\quad$ 0.5 $\quad$ 0.8 $\quad$ 0.8 $\quad$ 0.9

Fe XIII $\qquad$ T_e $\quad$ 1.8 $\times 10^6$ K

$\qquad$ $3s^2\ 3p^2\ \begin{array}{l}^3P_1 \\ ^1D_2\end{array} - 3s3p^3\ \begin{array}{l}^3P_2 \\ ^3P_2\end{array}$ $\quad$
311.549 $\quad$ 0.8 $\quad$ 1.0 $\quad$ 1.0 $\quad$ 1.0
354.345 $\quad$ 0.8 $\quad$ 1.0 $\quad$ 1.0 $\quad$ 1.0

Si XI $\qquad$ T_e $\quad$ 1.8 $\times 10^6$ K

$\qquad$ $2s^2\ ^1S_0 - 2s2p\ ^1P_1$ $\qquad$ 303.317 $\quad$ 1.0 $\quad$ 1.0 $\quad$ 1.0 $\quad$ 1.0

Fe XIV $\qquad$ T_e $\quad$ 2.0 $\times 10^6$ K

$\qquad$ $3s^2\ 3p\ \begin{array}{l}^2P_{3/2} \\ ^2P_{3/2}\end{array} - 3s3p^2\ \begin{array}{l}^2S_{1/2} \\ ^2D_{5/2}\end{array}$ $\quad$
289.169 $\quad$ 0.7 $\quad$ 0.7 $\quad$ 1.0 $\quad$ 1.0
353.847 $\quad$ 3.1 $\quad$ 1.4 $\quad$ 1.0 $\quad$ 1.0

S XII $\qquad$ T_e $\quad$ 2.0 $\times 10^6$ K

$\qquad$ $2s^2\ 2p\ \begin{array}{l}^2P_{3/2} \\ ^2P_{1/2}\end{array} - 2s2p^2\ \begin{array}{l}^2D_{5/2} \\ ^2D_{3/2}\end{array}$ $\quad$
299.536 $\quad$ 2.5 $\quad$ 1.5 $\quad$ 1.1 $\quad$ 1.0
288.416 $\quad$ 0.7 $\quad$ 0.7 $\quad$ 0.9 $\quad$ 1.0

S XIII $\qquad$ T_e $\quad$ 2.5 $\times 10^6$ K

$\qquad$ $2s^2\ ^1S_0 - 2s2p\ ^1P_1$ $\qquad$ 256.700 $\quad$ 1.0 $\quad$ 1.0 $\quad$ 1.0 $\quad$ 1.0

Fe XV $\qquad$ T_e $\quad$ 2.5×10^6 K

$\quad$ $3s^2\ ^1S_0 - 3s3p\ ^1P_1$ $\qquad$ 284.17 $\quad$ 0.9 $\quad$ 0.9 $\quad$ 1.0 $\quad$ 1.0

Ar XIII $\qquad$ T_e $\quad$ 2.7×10^6 K

$\quad$ $2s^2 2p^2\ ^3P_2 - 2s2p^3\ ^3D_3$ $\qquad$ 248.665 $\quad$ 5.9 $\quad$ 2.0 $\quad$ 1.0 $\quad$ 0.9
$\qquad\quad\ ^3P_1 \qquad\qquad\ ^3D_2$ $\qquad$ 242.229 $\quad$ 3.4 $\quad$ 1.1 $\quad$ 0.9 $\quad$ 0.8
$\qquad\quad\ ^3P_1 \qquad\qquad\ ^3D_1$ $\qquad$ 241.915 $\quad$ 0.6 $\quad$ 0.5 $\quad$ 0.8 $\quad$ 0.8
$\qquad\quad\ ^3P_0 \qquad\qquad\ ^3D_1$ $\qquad$ 236.267 $\quad$ 0.6 $\quad$ 0.5 $\quad$ 0.8 $\quad$ 0.8

Fe XVI $\qquad$ T_e $\quad$ 3.2×10^6 K

$\quad$ $3s\ ^2S - 3p\ ^2P_{3/2}$ $\qquad$ 335.40 $\quad$ 1.0 $\quad$ 1.0 $\quad$ 1.0 $\quad$ 1.0
$\qquad\ ^2S \qquad\quad\ ^2P_{1/2}$ $\qquad$ 360.76 $\quad$ 1.0 $\quad$ 1.0 $\quad$ 1.0 $\quad$ 1.0

Ar XVI $\qquad$ T_e $\quad$ 4.5×10^6 K

$\quad$ $2s\ ^2S_{1/2} - 2p\ ^2P_{3/2}$ $\qquad$ 353.80 $\quad$ 1.0 $\quad$ 1.0 $\quad$ 1.0 $\quad$ 1.0

Ni XVIII $\qquad$ T_e $\quad$ 5.5×10^6 K

$\quad$ $3s\ ^2S_{1/2} - 3p\ ^2P_{1/2}$ $\qquad$ 320.55 $\quad$ 1.0 $\quad$ 1.0 $\quad$ 1.0 $\quad$ 1.0
$\qquad\ ^2S_{1/2} \qquad\quad\ ^2P_{3/2}$ $\qquad$ 291.98 $\quad$ 1.0 $\quad$ 1.0 $\quad$ 1.0 $\quad$ 1.0

Ca XVII $\qquad$ T_e $\quad$ 6.3×10^6 K

$\quad$ $2s2p\ ^3P_2 - 2p^2\ ^3P_1$ $\qquad$ 244.06 $\quad$ 1.0 $\quad$ 1.3 $\quad$ 2.0 $\quad$ 1.4
$\qquad\quad\ ^3P_2 \qquad\qquad\ ^3P_2$ $\qquad$ 232.83 $\quad$ 2.4 $\quad$ 6.2 $\quad$ 4.6 $\quad$ 1.6

Ca XVIII $\qquad$ T_e $\quad$ 7×10^6 K

$\quad$ $2s\ ^2S_{1/2} - 2p\ ^2P_{1/2}$ $\qquad$ 344.80 $\quad$ 1.0 $\quad$ 1.0 $\quad$ 1.0 $\quad$ 1.0
$\qquad\ ^2S_{1/2} \qquad\quad\ ^2P_{3/2}$ $\qquad$ 302.22 $\quad$ 1.0 $\quad$ 1.0 $\quad$ 1.0 $\quad$ 1.0

Fe XXI $\qquad$ T_e $\quad$ 1.2×10^7 K

$\quad$ $2s^2 2p^2\ ^3P_1 - 2s^2 2p^2\ ^1S_0$ $\qquad$ 330.23

Fe XXII $\qquad$ 1.3×10^7 K

$\quad$ $2s^2 2p\ ^2P_{1/2} - 2s2p^2\ ^4P_{3/2}$ $\qquad$ 292.48 $\quad$ 1.0 $\quad$ 1.0 $\quad$ 1.0 $\quad$ 1.0

Fe XXIII $\qquad$ T_e $\quad$ 1.5×10^7 K

$\quad$ $2s^2\ ^1S_0 - 2s2p\ ^3P_1$ $\qquad$ 263.7 $\quad$ 1.0 $\quad$ 1.0 $\quad$ 1.0 $\quad$ 1.0

Fe XXIV $\qquad$ T_e $\quad$ 3.0×10^7 K

$\quad$ $2s\ ^2S_{1/2} - 2p\ ^2P_{1/2}$ $\qquad$ 255.11 $\quad$ 1.0 $\quad$ 1.0 $\quad$ 1.0 $\quad$ 1.0
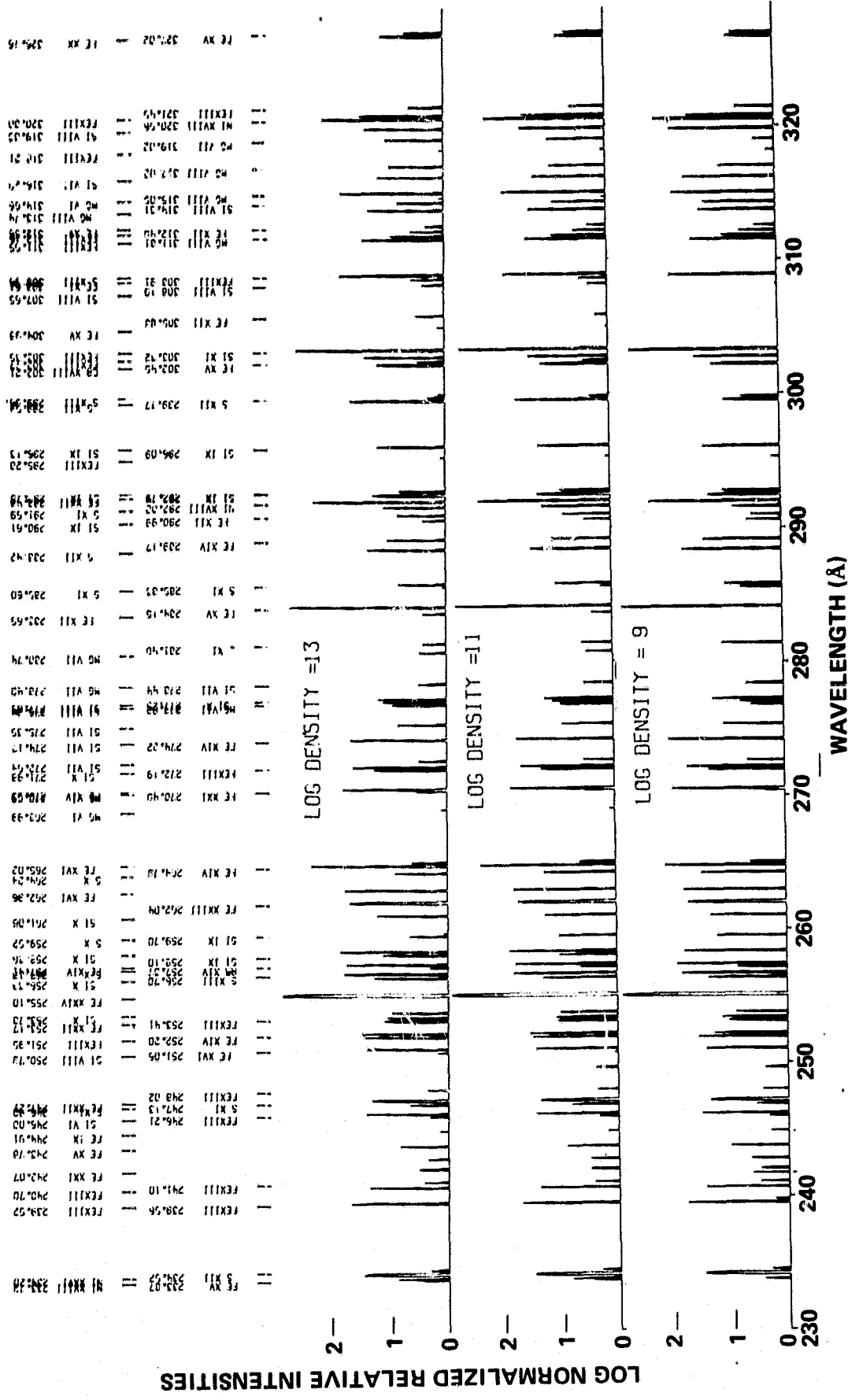
AII. Synthesized Solar Spectra Showing Changes in Line Strengths as Functions of Ambient Electron Density.

AIII.   EUV CAMERA DESIGN

Even though the design minimizes charge build-up, some will still occur and spark discharges must be prevented. Toward this end the film platen, dancers and guide idlers will be made of teflon or covered with the same estar base used for the film. The guide idlers will limit vertical motion of the film (perpendicular to the direction of dispersion) and will touch the film only on its edges. The supply and take-up reels will be made of gold-plated aluminum and carefully grounded to the baseplate allowing slow bleed-off of any accumulated charges. Sharp points and edges are avoided and clearance of about 5mm is provided between the film and any interior surfaces of the camera. Although black anodized aluminum has been used successfully with EK 101-07 film,[1] based on the laboratory experience of one of us,[2] we have decided to gold-plate all interior metallic camera surfaces.

The spectrograph focal surface is cylindrically concave to the incoming radiation and the film must conform to it within $\pm$ 0.2 mm. This is achieved by pressing the back side of the film against a platen with a hold-down mask having a 1.8 x 7 cm rectangular hole to allow the EUV photons to strike the emulsion. During transport of the film between exposures neither the platen nor the mask touch it and it appears as a chord cutting the focal curve. Once motion stops, the hold-down mask is driven against the platen (with the film between) by a linear solenoid and held there by a permanent magnet. At this point, power is removed from the normally-applied motor brakes[3] and then from the motors. The small increase in length between the chord and the focal arc defined by the platen is made up by the dancer springs (see below); the film is not stretched. Upon completion of an exposure, the hold-down mask is pulled away from the film and platen by a second solenoid and held away by a spring.

To minimize charge transfer, the platen and mask surfaces that contact the film will have estar film base material laminated to them. In spite of such precautions, touching the emulsion with the hold-down mask introduces the major complication of pressure induced film blackening. However, the pressure will be light ($\lesssim 0.51 b/in^2$) and any blackening is expected to be restricted to the contact areas more than 4mm from the recorded spectra.

The inertia of reels large enough to accommodate 600 ft. of EK 101-07 film, in conjunction with the film speed needed to give a 2s frame advance time would result in excessive film tension if only one drive were used. Therefore, the supply and take-up reels each has a drive and their relative speeds are servo-controlled, avoiding large film tensions during starting and stopping and as transfer of film from one reel to the other alters inertias and tangential velocities. A detailed servo analysis[4] performed on an equivalent lumped spring-inertia model of the camera (Figs. AIII-1 and AIII-2) demonstrates that the camera will operate smoothly with 225 ft. total film footage[5] regardless of the amount of film on each reel.

The diagram to the left of Figure AIII-1 shows the camera model that formed the basis of the servo-analysis. The two springs act against the film tension and minimize variation in it during acceleration, transport, and deceleration. The upper graph of the figure shows that although tension in the springs and the film does vary, it never gets large and the oscillation quickly damps out (because of the difference in lever arms, the film tension is about half that

LUMPED SPRING-INERTIA EQUIVALENT MODEL OF CAMERA

SPRING k_3 HAS A
PRELOAD DEFLECTION
EQUAL TO b_1

SPRING k_4 HAS A
PRELOAD DEFLECTION
EQUAL TO b_2

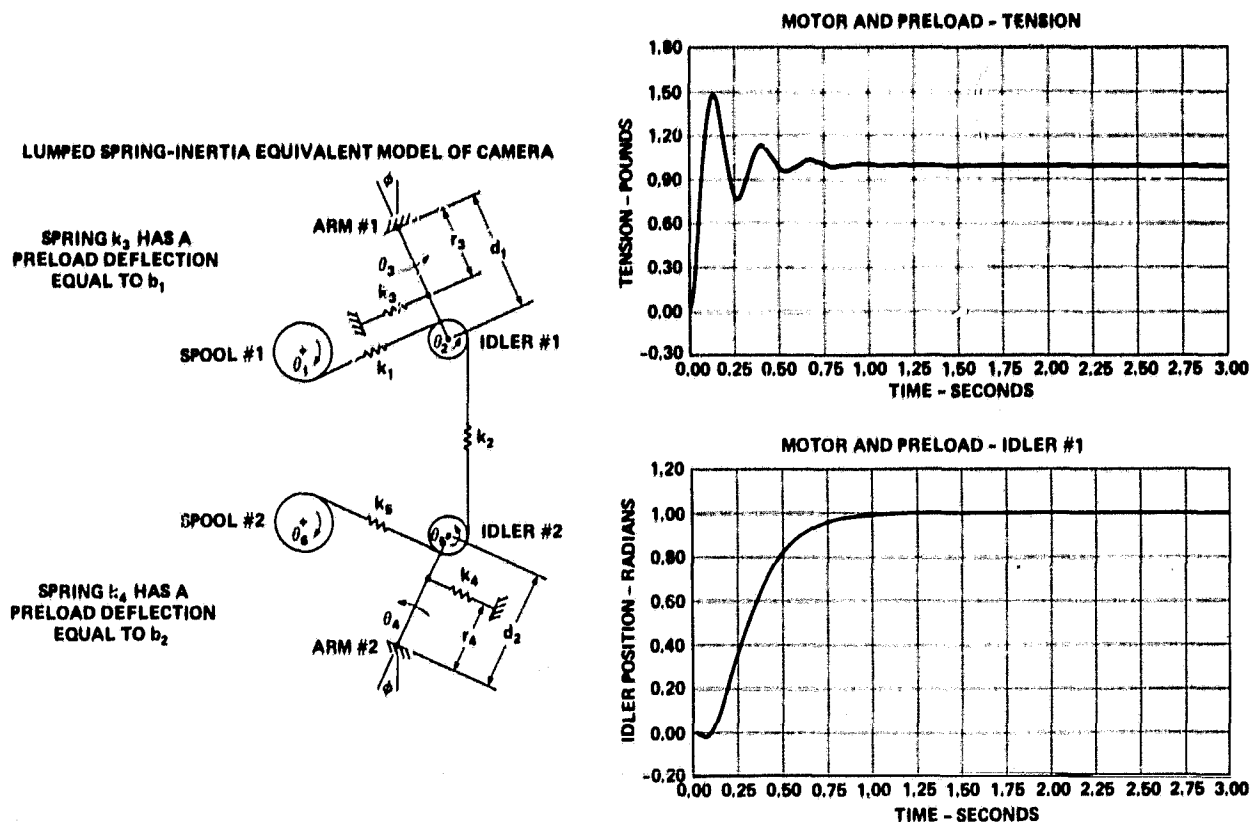MOTOR AND PRELOAD - TENSION

MOTOR AND PRELOAD - IDLER #1

Figure AIII-1.   EUV Camera Servo Analysis.

shown). Indeed, in the actual camera, damping due to the film itself will prevent even this small fluctuation. The lower graph of the figure shows that rotation of the idler(s), and hence the motion of the film, is smooth and is completed in a second.

Figure AIII-2 gives the block-flow diagram for the servo-analysis. A command filter (at upper left) slows the response of the camera servo, moderating the motor current surges and preventing impulsive jerking of the film. A film footage indicator keyed to the rotation of idler #1, provides the signal used to compute gain G_1 appropriate to the reel inertias of the moment.

AIV.   AN AID FOR SEUTS

A photoelectric imaging detector for solar coronal observations must meet stringent requirements. It needs __many__ resolution elements (pixels) in order to provide high resolution with reasonable spectral and spatial coverage (e.g., 2nm spectral range at 0.005nm resolution x 6 arcmin FOV at 2 arcsec resolution $\Longrightarrow$ 70,000 pixels. Rastering systems give up too much in temporal resolution meeting this requirement to be acceptable. The detector's
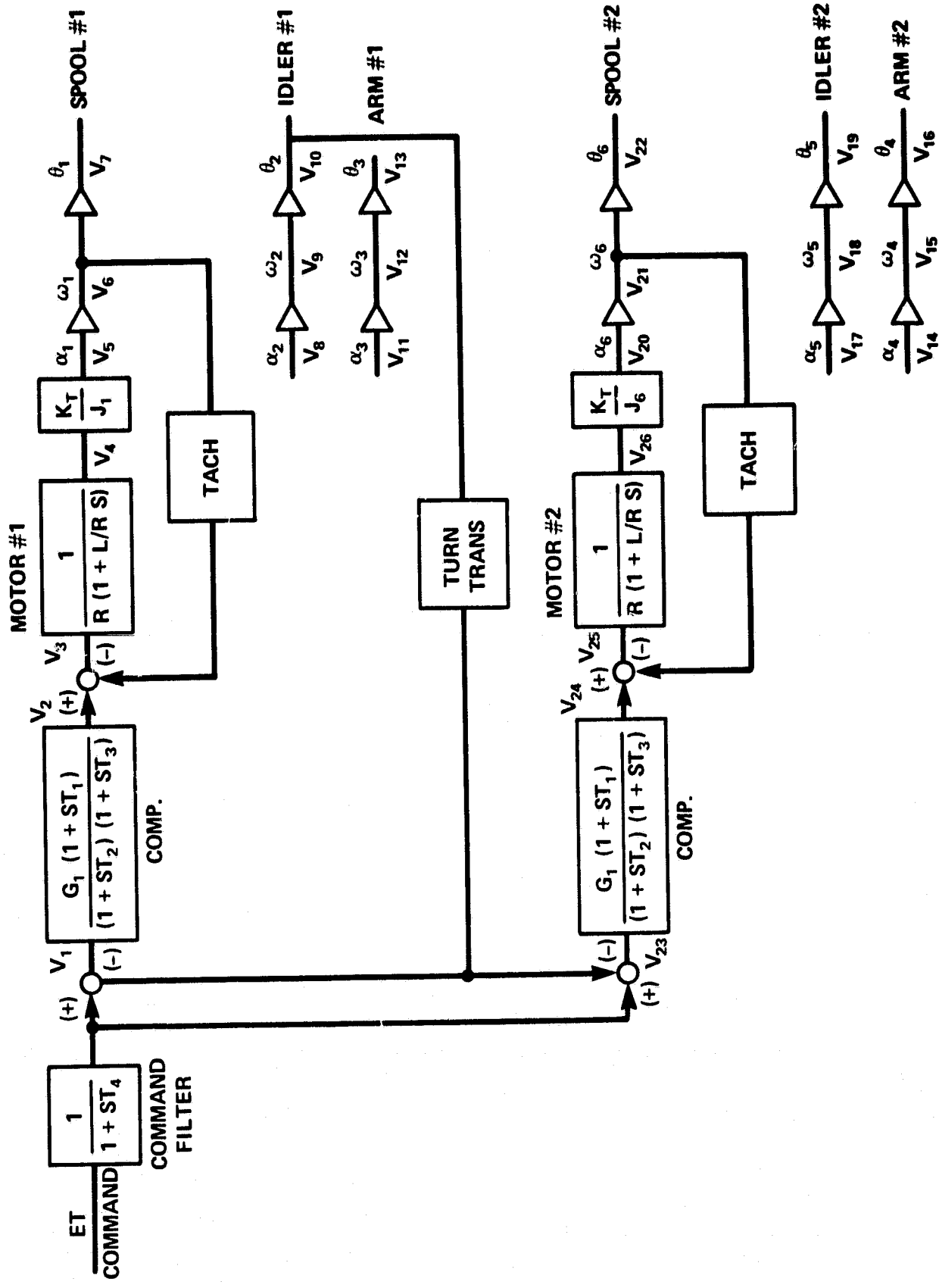
Figure AIII-2. Block Diagram of Camera Servo System.

Table AIV-1 Detector Trade-off[*]

	Digicon	Ranicon	MCP/SSA	PFD	SEUTS/Science Requirements
Format	1×512[a]	$1\ cm \times 1\ cm$	328×488[b]	328×488	200 spatial x 500 spectral
Resolution Element	$45\ \mu m \times 45\ \mu m$	1 part in 350 of length[c]	$23\ \mu m \times 23\ \mu m$	$46\ \mu m \times 46\ \mu m$	$45\ \mu m \times 20\ \mu m$
Estimated MTF[d] at 10 p/mm	60%	95%	39%	37%	at least 33%
15 p/mm	24%	76%	26%	12%	at 10 p/mm
20 p/mm	3%	50%	12%	2%	
Max. Temporal Res (s)	0.1	$(10^{-5}-10^{-6})$[f]	2.0[g]	2.0	2.0
Min. Dead Time (s)	0.05	3×10^{-5}	0.854	0.854	0.854
Observable Brightness (Photon/s-cm²-res. el.) Minimum (sensitivity)	(1.3×10^{3})[h]	5	5	5	10^{4}
Maximum (saturation)	1.3×10^{6}	4×10^{6}	6.5×10^{9}	(1.3×10^{9})[i]	10^{9}
Dynamic Range/res. el. - exposure	10^{3}	8×10^{5}	6.1×10^{2}	(2.6×10^{3})[k]	10^{5}
Detective Quantum Eff	~ 0.75 RQE[j] (mesh photocathode)	~0.75 RQE (photoemissive matl. in MCP pores)	~0.25 RQE (Photoemissive matl. in MCP pores)	~0.75 RQE (mesh photocathode)	as high as possible
Vacuum Requirement	Good Vacuum	Hard Vacuum	Hard Vacuum	Poor Vacuum	Poor Vacuum
Voltage Required	20 kV	2 kV	7 kV	7 kV	
Availability	Good	Need development for 2-dimensional detection	commercial components available	components available	
General	40 cm long x 3 cm dia., ~22 kg	light weight, simple	complex	lightweight simple	

[*] see list of references for notes to this table

sensitivity and detective quantum efficiency (DQE) should be high, preferably
enough for single photon detection. Its dynamic range should be large so as
to handle the large range of solar coronal intensities and its saturation level
should be adequate for the expected focal plane photon densities (see Table III-2).
The open structure necessitated by the EUV wavelengths (22.5-37.0nm) leads to
requirements for stable photocathode material and careful design to avoid arcing.

The Digicon, a device being used for the Space Telescope's High Resolution Spec-
trograph (HRS),[5] consists of a photocathode (which could be an open mesh structure[7]),
a magnetic stage to accelerate and reimage the photoelectrons, a linear array
of silicon diodes, and individual electronic channels for each diode. It is
a stable, multi-channel pulse-counting device[8] suitable for space flight. How-
ever, as can be seen from Table AIV-1, its number of resolution elements and
saturation level are inadequate for our requirements.

The Ranicon, a chevron-pair of microchannel plates (MCP's) feeding a resistive
anode target surface is a pulse-counting detector which has been successfully
used for rocket-borne astronomy.[9] A centroid measuring device, the Ranicon
is insensitive to beam spreading and has the potential for high spatial resol-
ution. However, only one dimensional detection has been implemented so far.
More importantly, the MCP's have to be run in the saturation mode in order to
supply electron bursts that are large enough.[10,11] This limits the focal plane
photon density that this detector could handle to only 4×10^6 photons/cm^2/s.
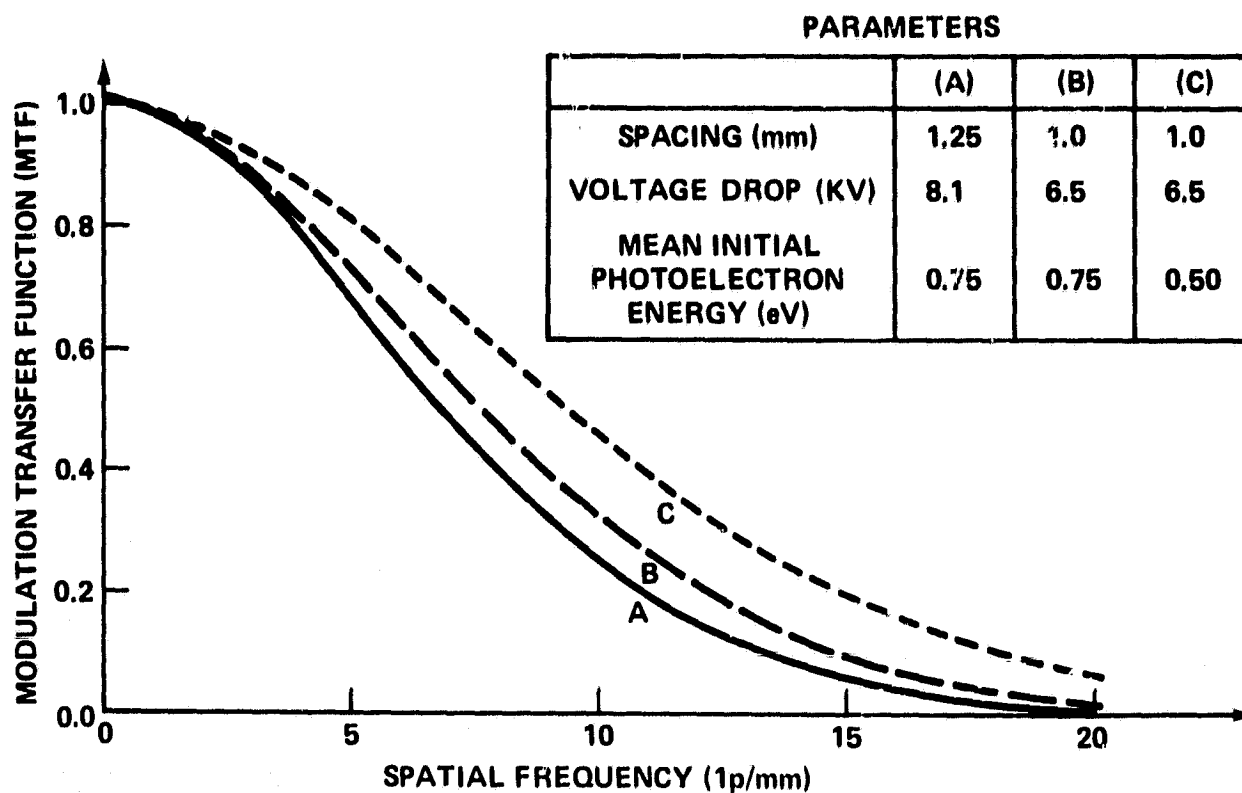
A detector system (MCP/SSA) constructed from commerically available parts would
use an MCP as the photocathode and gain element, an aluminized phosphor and
reimaging lens to convert the electron image into a visible one, and a self-
scanned array (SSA) such as a CCD for readout. However, the synthesized de-
tector system has never been constructed and space qualified. More critically,
the MCP must be operated at low gain in order to allow a reasonable dynamic
range[12] and this, unfortunately results in a quasi-exponential pulse height
distribution and poor DQE[13].

The proximity focused diode (PFD) that we favor would use a semi-transparent
electroformed mesh coated with photemissive material (e.g., Mg F$_2$) to detect
the EUV photon image, a moderate voltage drop ($\sim$ 6.5 kV) for acceleration and
focus, and a solid state array for readout (Figure 2e). A front bias ring
produces an electric field at the mesh strong enough to direct emitted photo-
electrons through the holes into the acceleration and focusing region[7]. The
open tube-structure allows rapid outgassing, easing the problem of attaining
the needed vacuum ($\sim 10^{-5}$ torr).

As the SSA-readout we will use the Texas Instrument 488 x 328 CCD being developed
for the Laboratory for Astronomy and Solar Physics at the GSFC. Its dark
current noise can be eliminated by cooling, and the floating gate amplifiers
and header design (developed for Jack Williams of this laboratory) result in
a total noise figure of < 100 charges/well-readout. A 6.5 kV electron will
produce $\sim$ 1250 electrons in a well of this back-side thinned CCD, giving a
signal-to-noise ratio of > 12 which is more than enough for single photon
detection.

Figure AIV-1 shows the modulation transfer function (MTF) estimated for a proxi-
mity focused diode[14] used at $\sim$ 30nm. It does not include the resolution loss
due to the CCD nor the focusing affect of the mesh photocathode.[15] The major
uncertainty in this calculation is the value of the mean initial photoelectron
energy. Based on a study of photoelectric effects in various alkali halides[16]

Figure AIV-1.   Estimated MTF for Proximity Focussed Diode.

PARAMETERS

	(A)	(B)	(C)
SPACING (mm)	1.25	1.0	1.0
VOLTAGE DROP (KV)	8.1	6.5	6.5
MEAN INITIAL PHOTOELECTRON ENERGY (eV)	0.75	0.75	0.50

we estimate this to be 0.5 - 0.75 eV for a Mg F_2 photocathode. The relatively poor spatial resolution of the PFD can be improved by the use of electrostatic or magnetic focusing, although at the cost of additional size, weight, and power.

AV.   DATA ACQUISITION FOR AID AND H-α MONITOR

To avoid the cost, volume, weight, and power penalties of including a space qualified buffer memory within the SEUTS, the instrument microprocessor will direct a CCD output (either from the AID or the H-α slit jaw monitor) through a common A/D convertor (further reducing costs, etc.) directly into the Spacelab High Rate Multiplexer (HRM) via a SEUTS dedicated line. The AID will integrate for 1.146s and the full CCD frame read out over 0.854s for a 2s cycle time. Every fifth cycle the CCD in the H-α monitor will be read out (at the same rate) instead of the AID CCD. We will use 8 bits/CCD-pixel for a 1.5 Mbps telemetry rate down to the POCC. Engineering and housekeeping data will be merged with the scientific data by the microprocessor and telemetered at the same rate down to the SEUTS' GSE.
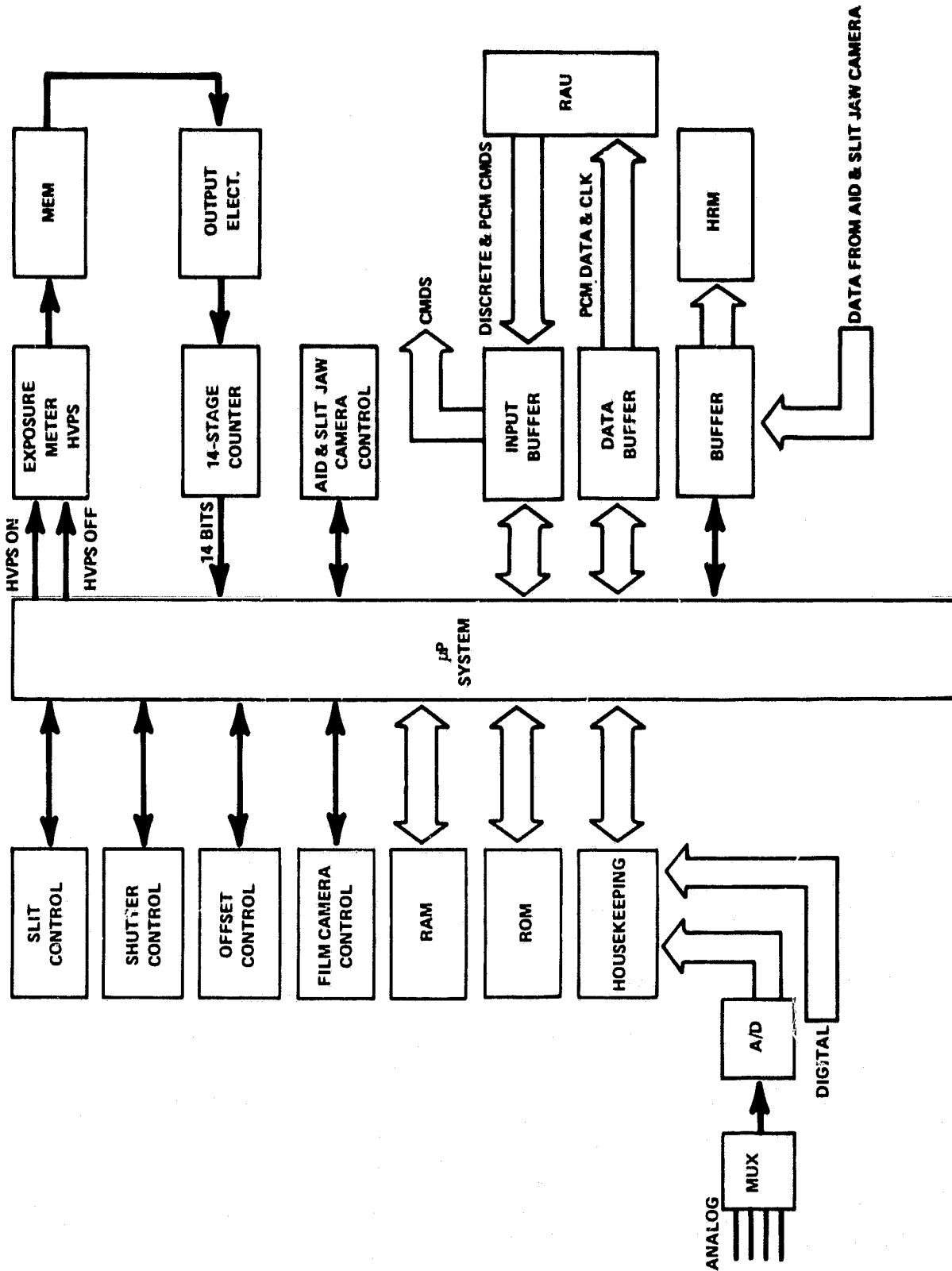
AVI.   Microprocessor System Block Diagram.

AVII.   SEUTS POINTING REQUIREMENTS

The SEUTS requires stabilization during all exposure sequences to the extent that no significant smearing should be introduced during an exposure   SEUTS resolution in the presence of IPS pointing errors is summarized in Table III-3.

TABLE III-3.   Effect of Pointer Errors on SEUTS Performance
(arcsec)

IPS Performance (σ)	SEUTS Resolution		Combined Resolution	
	FWHM	σ	FWHM	σ
1.0	2.0	0.85	3.1	1.31
0.33	2.0	0.85	2.1	0.91

Evidently, to achieve full SEUTS capability, the IPS should approach its "goal" performance of 0.33 arcsec. The performance should be held over a period of one exposure and, preferably, over a sequence of exposures in order that sequential observations of doppler line profiles for each point on the entrance aperture always correspond to the same structure on the sun.

Additional pointing requirements are:

1.   The pointing system must be able to orient the instrument to a desired point on the sun (and 0.5 degree above the solar limb) to a spatial accuracy of 10 arcsec. For special observing programs requiring orientation of the entrance aperture along a specific solar structure we will need to specify IPS roll orientation to 1 degree. Since IPS will probably carry a cluster of instruments, we request that prime IPS pointing be allocated to SEUTS on time-shared basis.
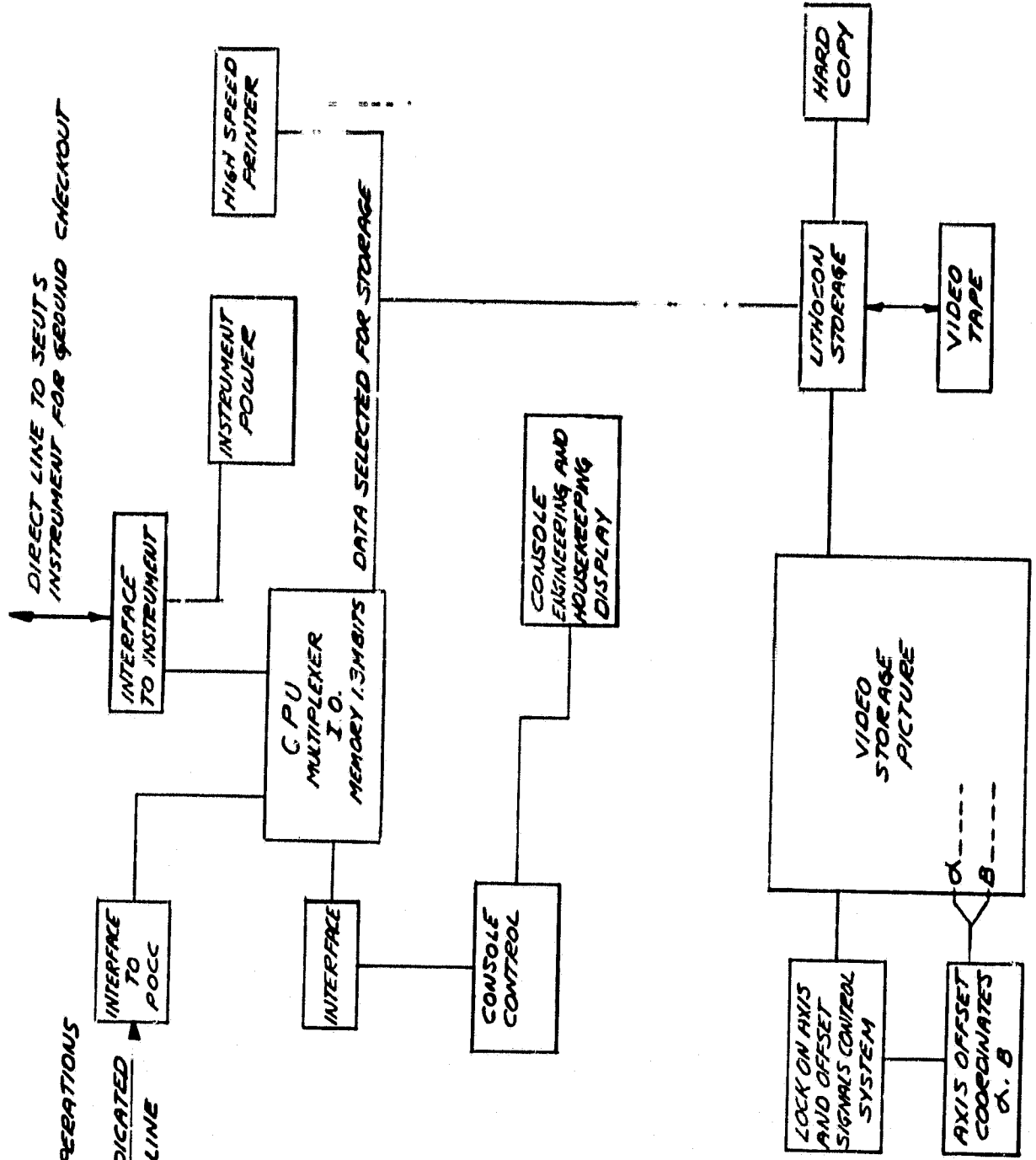
2.   It would be desirable for the pointing system to compensate for solar rotation of the location at the center of the EUV slit. (The proper motion of a point on the sun depends on its location on the solar disk).

3.   The pointing system should be able to move a specified increment (fixed when the interface is defined but probably 20 arcsec) between SEUTS photographic exposures in a time of no greater than 5s.

To derive maximum scientific benefit from a cluster of instruments, all but one instrument in the cluster should have independent offset capability to achieve realignment in space or to permit pointing to different portions of the sun simultaneously. We have studied various engineering options[17] and established that the EUV image cannot be internally scanned in an instrument such as SEUTS. We therefore request that, if at all possible, SEUTS be mounted directly to the IPS and have primary control of pointing direction. If this is not possible, an offset point system such as the CAS system on the SMM's UVSP can be implemented at extra cost. This system would provide one axis of rotation parallel to the long dimension of the entrance slit so that a 8 arcmin wide swath across the sun could be covered with changing IPS pointing (Requirement 3 would also be satisfied). IPS would be used for non-critical offset pointing adjustments in the orthogonal direction.

AVIII-1 GSE

FOR INSTRUMENT GROUND
CHECK OUT AND FLIGHT OPERATIONS

DIRECT LINE TO SEUTS
INSTRUMENT FOR GROUND CHECKOUT

SEUTS DEDICATED
DATA LINE

INTERFACE TO INSTRUMENT

INTERFACE TO POCC

HIGH SPEED PRINTER

INSTRUMENT POWER

CPU
MULTIPLEXER
I.O.
MEMORY 1.3 MBITS

DATA SELECTED FOR STORAGE

CONSOLE
ENGINEERING AND
HOUSEKEEPING
DISPLAY

INTERFACE

CONSOLE CONTROL

LITHOCON STORAGE

VIDEO TAPE

HARD COPY

VIDEO
STORAGE
PICTURE

α ----
B ----

LOCK ON AXIS
AND OFFSET
SIGNALS CONTROL
SYSTEM

AXIS OFFSET
COORDINATES
α, B

AVIII. PAYLOAD SPECIALIST SUPPORT--REAL TIME INSTRUMENT OPERATIONS FROM THE ORBITER

A. On-Board Displays Required

Displays required at the Aft Flight Deck (AFD) include video output from the SEUTS Hα slit jaw camera (updated every 10 sec) and two pages of status data (preferably one page displayed simultaneously with the Hα display) including EUV monitor output.

B. Target Selection and Mode Selection by the Payload Specialist

The SEUTS will have several observing routines pre-programmed and initiated by ground or AFD command using the Hα slit jaw monitor for target selection. Scientific value of the observations can be maximized if the payload specialist can enter new target coordinates in response to transient solar phenomena. He should also be able to "fine tune" the position of the SEUTS slit (i.e. changing the pointing direction), using an on-board controller to control pointing. This would be much more difficult to do from the ground.

C. Payload Specialist Time Required

The total burden SEUTS will place on the crew depends critically on the level of solar activity at flight time. At times of low activity the burden will be low, being mostly fine tunings of the slit position and alignment checks (using the Hα display and EUV monitor) with the IPS pointing sensor. Fifteen blocks of time in daylight, each about 15 minutes long, should be adequate to initiate from the AFD. If the level of activity is high, then heavier crew participation may be required in a flare search mode.

FLIGHT OPERATIONAL (NON-CREW) REQUIREMENTS

A. Special Interface Requirements

1. Pointing

Pointing requirements have been presented earlier. SEUTS can be operated as part of a cluster on IPS. However, individual pointing systems for each instrument would be highly desirable as it would permit concurrent observations on each instruments' prime targets.

2. High-Rate KU Band for Image Transmission

For photoelectric or Hα data readout the instrument will produce approximately 1.5 Mbps of data. This can be telemetered through the High Rate Multiplexer (HRM) using a channel dedicated to SEUTS.

B.   Orbital Requirements

SEUTS can operate in either high or low inclination orbits. A high altitude
(> 400 km) is desirable to minimize EUV absorption by the residual terrestrial
atmosphere

C.   Real-Time Ground Support Requirements

SEUTS real-time ground operations will require a set of ground support equipment (GSE)
used for both ground checkout and flight operations. All engineering data will
be merged with scientific data and down linked to the instrument's GSE. Commands
to the SEUTS will be sent from a POCC console.

1.   Ground Displays Required

It is necessary to display engineering and housekeeping data as well as the time-
shared Hα and EUV spectrum images in the POCC. All software and hardware necessary
to produce the displays will be a part of the instrument GSE- see Figure AVIII-1.

2.   Total Amount of Real-Time Operations Support Required from POCC

The amount of real-time operations from POCC depends on the amount of time
dedicated on the mission to solar observations and the availability of the pay-
load specialist to react to transient phenomena on the sun. Ideally, ground
operations will take place only for non-time critical observations, that is, for
observations of solar phenomenon such as a coronal holes where rapid reaction
to transient events is not required. Approximately 15 blocks of observation
will be initiated from the POCC. Typically, such observations will require
pointing commands and commands to start preplanned observing sequences. Real-
time operations are also required during initial turn-on of all high voltages
(EUV monitor and AID system).

POST-FLIGHT REQUIREMENTS

Upon touchdown the SEUTS camera must be cooled as quickly as possible, using
a ground purge system, to minimize film deterioration. The camera should be
stored in a cooled, controlled environment prior to delivery to the experimenter.

SECTION II REFERENCES

1. W. M. Neupert, Y. Nakagawa, and D. M. Rust, Solar Phys., 43, 359-376 (1975).

2. P. V. Foukal, Astrophys. J., 210, 575-581 (1976).

3. J. A. Vorpahl, E. Tandberg-Hanssen, and J. B. Smith, Jr., Astrophys. J., 212, 550-560 (1977).

4. R. H. Levine and G. L. Withbroe, Solar Phys., 51, 83-101 (1977).

5. A. S. Krieger, Proceedings of the OSO-8 Workshop, Boulder, Colorado, November 7-10, 1977, pp. 98-122.

6. R. Rosner, L. Golub, B. Coppi, and G. S. Vaiana, Astrophys. J., 1978, in press.

7. D. G. Wentzel, Solar Phys., 39, 129-140 (1974).

8. D. G. Wentzel, Solar Phys., 50, 343-360 (1977).

9. J. A. Ionson, Astrophys. J., 226, 1978, in press.

10. M. Kuperus, Space Sci. Rev., 9, 713-739 (1969).

11. D. S. Spicer, Solar Phys., to be published.

12. A. A. Galeev, preprint, Harvard-Smithsonian Center for Astrophysics.

13. P. V. Foukal, Astrophys. J., 223, 1046-1057 (1978).

14. J. B. Zirker, Rev. Geophys. Space Phys., 15, 257-269 (1977).

15. W. M. Neupert and V. Pizzo, Journ. Geophys. Res., 79, 3701-3709 (1974).

16. M. D. Altschuler, D. E. Trotter, and F. Q. Orrall, Solar Phys., 26, 354-365 (1972).

17. R. H. Munro and B. V. Jackson, Astrophys. J., 213, 874-886 (1977).

18. R. H. Levine, M. D. Altchuler, and J. W. Harvey, J. Geophys. Res., 82, 1061-1065 (1977).

19. W. M. Adams and P. A. Sturrock, Astrophys. J., 202, 259-264 (1975).

20. R. A. Kopp and T. E. Holzer, Solar Phys., 49, 43-56 (1976).

21. R. A. Kopp and F. Q. Orrall, Astr. Ap., 53, 363-375 (1976).

22. R. Rosner and G. S. Vaiana, Astrophys. J., 216, 141-157 (1977).

23. G. Cushman and W. A. Rense, Astrophys. J. (Lett.) 207, L61-L62 (1976); 211, L57 (1977).

24. R. J. Thomas, unpublished work.

25. A. S. Krieger, Proceedings of the OSO-8 Workshop, Boulder, Colorado, November 7-10, 1977, pp. 98-122.

26. N. R. Sheeley, J. D. Bohlin, G. E. Brueckner, J. D. Purcell, V. Scherrer, and R. Tousey, Solar Phys. 40, 103-121 (1975).

27. G. E. Brueckner, J.-D. F. Bartoe, M. E. VanHoosier, Proceedings of the OSO-8 Workshop, Boulder, Colorado, November 7-10, 1977, pp. 380-418.

28. J. E. Vernazza, P. V. Foukal, M. C. E. Huber, R. W. Noyes, E. M. Reeves, E. J. Schmahl, J. G. Timothy, and G. L. Withbroe, Astrophys. J. (Lett.) 199, L123-L126 (1975).

29. G. L. Withbroe, Proceedings of the OSO-8 Workshop, Boulder, Colorado, November 7-10, 1977, pp. 2-27.

30. J. T. Mariska, U. Feldman, and G. A. Doschek, Astrophys. J., to be published.

31. C. Jordan, Mon. Not. R. Astr. Soc. 170, 429-440 (1975).

32. J. L. Linsky, D. L. Glackin, R. D. Chapman, W. M. Neupert, and R. J. Thomas, Astrophys. J. 203, 509-520 (1976).

33. D. L. Glackin, J. L. Linsky, S. A. Mango, and J. D. Bohlin, Astrophys. J. 222, 707-715.

34. U. Feldman, G. A. Doschek, M. E. VanHoosier, and R. Tousey, Astrophys. J. (Lett.) 199, L67-L70 (1975).

35. J. L. Kohl, Astrophys. J. 211, 958-965 (1977).

36. G. L. Epstein and R. Steinitz, BAAS 7, 450-451 (1975); BAAS 7, 522-523 (1975).

37. E. G. Chipman, Proceedings of the OSO-8 Workshop, Boulder, Colorado, November 7-10, 1977, pp. 357-364; Astrophys. J. 224, 671-676 (1978).

38. E. C. Bruner, Jr., Proceedings of the OSO-8 Workship, Boulder, Colorado, November 7-10, 1977, pp. 427-441.

39. R. D. Chapman, S. D. Jordan, W. M. Neupert, and R. J. Thomas, Astrophys. J. (Lett.) 174, L97-L99 (1972).

40. W. M. Neupert, M. Swartz, and S. O. Kastner, Solar Phys. 31, 171-195 (1973).

41. I. J. D. Craig, Solar Phys. 31, 197-205 (1973).

42. S. O. Kastner, W. M. Neupert, and M. Swartz, Astrophys. J. 191, 261-270 (1974).

43. K. P. Dere, Astrophys. J. 221, 1062-1067 (1978).

44. G. A. Doschek, U. Feldman, and K. P. Dere, Astron. Astrophys. (Lett.) 60, L11-L13 (1977).

45. H. E. Mason, G. A. Doschek, U. Feldman and A. K. Bhatia, Astron. Astrophys. to be published.

46. U. Feldman, G. A. Doschek, and K. G. Widing, NRL preprint, to be submitted.

SECTION III REFERENCES

1. S. O. Kastner and H. E. Mason, Astron. Astrophys. 67, 119-127 (1978).

2.   C. C. Cheng, G. A. Doschek, and U. Feldman, Astrophys. J., to be published.

3.   G. D. Sandlin, G. E. Brueckner, and R. Tousey, Astrophys. J. 214, 898-904 (1977).

4.   M. C. E. Huber, A. K. Dupree, L. Goldberg, R. W. Noyes, W. H. Parkinson, E. M. Reeves, and G. L. Withbroe, Astrophys. J. 183, 291-312 (1973).

5.   E. M. Reeves, J. G. Timothy, M. C. E. Huber, and G. L. Withbroe, Appl. Opt. 16, 837-848 (1977).

6.   D. L. Garrett, J. D. Purcell, and R. Tousey, Astron. J. 69, 147-148 (1964) abs.

7.   R. Tousey, J.-D. F. Bartoe, G. E. Brueckner, and J. D. Purcell, Appl. Opt. 16, 870-878 (1977).

8.   J. D. Mangus, Appl. Opt. 9, 1019-1025 (1970).

9.   U. Feldman, G. A. Doschek, D. K. Prinz, and D. J. Nagel, J. Appl. Physics 47, 1341-1350 (1976).

10. T. Namioka, M. Seya, and H. Noda, Japanese Journal of Applied Physics 15, 1181-1197 (1976).

11. M. E. VanHoosier, J.-D. F. Bartoe, G. E. Brueckner, N. P. Patterson, and R. Tousey, Appl. Opt. 16, 887-892 (1977).

12. Conceptual Study for A Solar XUV Facility, Astronomy Spacelab Payloads Project, prepared by Ball Brothers Research Corporation, Boulder, Colorado, GSFC X-682-76-102.

13. G. A. Doschek, U. Feldman, M. E. VanHoosier, and J.-D. F. Bartoe, Astrophys. J. Suppl. 31, 417-443 (1976).

14. G. A. Doschek, U. Feldman, M. E. VanHoosier, and J. D. Purcell, Astrophys. J. Suppl. 31, 445-466 (1976).

15. S. A. Mango, J. D. Bohlin, D. L. Glackin, and J. L. Linsky, Ap. J., 220, 683-691 (1978).

16. J. Reader, G. L. Epstein and J. O. Ekberg, J. Opt. Soc. Am., 62, 273-284 (1972).

17. L. N. Kippel, Adv. in X-Ray Analysis 18, p. 146-158 (1974).

18. W. M. Burton, A. T. Hatter, and A. Ridgeley, Appl. Opt. 12, 1851-1857 (1973).

19. J. Osantowski, J. Opt. Soc. Am. 64, 834 - 838, 1974.

20. ORI Study of Detector Selection and Data System Requirements for a Solar Coronal XUV Shuttle Experiment, Technical Report 1351A, NAS 5-23438 (1978).

21. G. R. Carruthers, Appl. Opt. 14, 1667-1672 (1975).

22. G. E. Brueckner, J.-D. F. Bartoe, and M. E. VanHoosier, Proceedings of the OSO-8 Workshop, pp. 380-418 (1977).

APPENDIX REFERENCES AND NOTES

1. M. E. VanHoosier, J.-D. F. Bartoe, G. E. Brueckner, N. P. Patterson, and R. Tousey, Appl. Opt. 16, 887-892 (1977).

2. Dr. Uri Feldman of the Naval Research Laboratory and his colleagues there have extensive experience using Schumann film in a small roll-film camera (see Reference 9-Section III).

3. The D.C. tachometer-torque motors have been sized to override the electronic brakes in the event that they fail. The penalty would be increased power drain and somewhat slower film advance.

4. Design and Analysis of a Roll-Film Camera for the EUV, in progress by General Electric.

5. The present analysis has been carried out for a film footage of 225 ft. because that is the maximum that Eastman Kodak will manufacture. However, it is expected that camera operation will not be appreciably degraded by use of the full 600 ft. capacity. More uniform film quality can be guaranteed by Eastman Kodak if it is manufactured in 100 ft. strips and we are now pursuing methods of splicing Schumann film.

6. "A High Resolution Spectrograph for the Space Telescope, Part II Technical Description," Goddard Space Flight Center, HRS-680-77-01.

7. G. A. Carruthers, Appl. Opt. 14, 1667-1672 (1975).

8. R. G. Tull, J. P. Choisser, and E. H. Snow, Appl. Opt. 14, 1182-1189 (1975).

9. H. Weiser, R. C. Vitz, H. W. Moos, and A. Weinstein, Appl. Opt. 15, 3123-3130 (1976).

10. M. Lampton and F. Paresce, Rev. Sci. Instrum. 45, 1098-1105 (1975).

11. J. G. Timothy and R. L. Bybee, Appl. Opt. 14, 1632-1644 (1975).

12. "A Study of Detector Selection and Data System Requirements for a Solar Coronal XUV Shuttle Experiment," prepared for NASA/GSFC by ORI, TR 1351 and 1351A, NASA 5-23438 (1978).

13. B. W. Manley, A. Guest, and R. T. Holmshaw, Adv. Electron. Electron Phys. 28A, 471-486 (1969).

14. J. Goodson, A. J. Woolgar, J. Higgins, and R. F. Thumwood, Adv. Electron. Electron Phys. 33A, 83-92 (1972).

15. Communication with G. R. Carruthers; pulling the photoelectrons through the interstices of the mesh results in a more forward directed angular distribution than Lambertian. However, as discussed in Reference 7 of this Appendix, a sensor using a mesh photocathode must be slightly defocused.

16. J. W. Taylor and P. L. Hartman, Phys. Rev. 113, 1421-1435 (1969).

17. BBRC Independent Rastering Study, Report 76-24, NAS 5-23402 (1959)

Footnotes to Table AIV-1.

a) Saddle deflection coils orthogonal to optic axis allow raster scanning of the entire photocathode area by the target diode array.

b) Based on choosing the Texas Instrument CCD (Table AIV-2).

c) A resolution of 1 part in 500 appears reasonable for one dimensional detection. Since the accuracy depends on the size of the charge packet which would be divided between the two dimensions, we take $500/\sqrt{2}$ for the two dimensional case.

d) No distinction is made between MTF and Square Wave Amplitude Response (SWAR) in these rough estimates.

e) The limiting spatial frequency is (1/P) rather than (1/2P) (where P is the pitch of the array pixel) because the image can be scanned across the target array (see note a).

f) Determined by available electronics and degree of confusion acceptable.

g) Fixed by the number of bits/CCD-pixel desired and telemetry rate to be employed (see Appendix AV).

h) Based on estimated dark count rate (counts/s res. el.) outside the South Atlantic Anomaly (SAA).

i) Inversely proportional to the integration time up to a maximum set by the photocathode.

j) Responsive Quantum Efficiency of the photocathode.

k) The dynamic range (for a single point EUV image) benefits from the spatial resolution. If electrostatic or magnetic focusing is used to improve it, the dynamic range/resolution element/exposure becomes $650 \times N_{eff}$ where N_{eff} is the number of CCD wells corresponding to the PFD resolution element.

INSTRUMENT FACT SHEETS
AO-OSS-2-78

DATE FILLED OUT Nov. 8, 1978

TITLE OF INVESTIGATION A Solar Extreme Ultraviolet Telescope and Spectrograph for Shuttle

PRINCIPAL INVESTIGATOR

NAME   Werner M. Neupert

ADDRESS   Laboratory for Astronomy and Solar Physics
Code 682
NASA, Goddard Space Flight Center
Greenbelt, Md., 20770

PHONE NUMBER 301-982-5523

FLIGHT INTEREST (Spacelab or LDEF) Spacelab

SCIENCE OBJECTIVE CATEGORY

_____	**Astronomy**
_____	**Relativity**
_____	**Upper Atmospheric Physics**
_____	**Comparative Planetary Atmospheres**
_____	**Space Plasma Physics**
X	**Solar Physics**
_____	**High Energy Astrophysics**
_____	**Planetary Physics and Chemistry**

I.   SUMMARY OF INVESTIGATION

This proposal outlines a scientific investigation that addresses several fundamental problems of solar physics:

o   The energy and mass balances in closed magnetic field regions in the corona and the processes by which these regions are heated.

o   Mass and energy transport into the solar wind.

o   The characteristics of the emergence and evolution of coronal active regions and their relation to flare activity and coronal holes.

An investigation of these problems requires observations with high spectral resolution simultaneously over the range of solar temperatures from 1×10^5 to 2×10^7 K, and over an extended field of view. The required observations are most effectively obtained in the extreme ultraviolet but no adequate data have been obtained to date. No instrument available on the Solar Maximum Mission or currently being developed for Spacelab 1 or 2 can make such measurements. Thus, we propose to construct and use a solar extreme ultraviolet telescope and spectrograph (SEUTS) for the Spacelab program.

The instrument proposed is a novel combination of existing technologies that most effectively provides the needed EUV data. A grazing incidence telescope with high EUV reflectivity feeds a diffraction grating at near normal incidence. The grating, ruled on a toroidal surface, not only spectrally disperses the radiation but also images each point of the spectrometer's entrance aperture onto a small spot in the focal plane so that spatial information is preserved. Adequately stigmatic images are produced over an 8 arcmin long slit and over a spectral range of 22.5 to 37.0nm. This is the most effective, narrow range of wavelengths containing emission lines sensitive to the temperature range that must be observed. Schumann-type photographic film is used to gain the full performance of the optical system. Spatial resolution of at least 2 arcsec and spectral resolution of 0.005nm is achievable throughout the central 4 arcmin field of view at all wavelengths with even better performance in the Rowland plane.

Recognizing that rapid solar phenomena cannot be fully investigated with a footage-limited film system, we also propose to carry and operate an open-mesh photocathode intensified CCD detector for engineering evaluation on the first flight. This offers an opportunity to evaluate such parameters as operation (and possible degradation) in the orbiter environment, detector stability during the extended integration period and sensitivity to the high energy particle environment of the orbiter. Observations will be made over a restricted wavelength range of 33.5 - 35.7nm and results will guide more extended use of such detectors in the prime focal plane on future missions.

II. STATUS OF INSTRUMENTATION

A. Check below to indicate the status of instrument design:

_____ Most elements of the instrumentation exist only as conceptual designs.

__X__ Designs exist for most of the instrumentation, but major elements have yet to be breadboarded and tested.

_____ Proven designs exist for all critical elements of the instrumentation.

_____ Other, describe _____
_____
_____
_____

B. Check below to indicate the status of instrument flight hardware:

__X__ Flight hardware development not yet begun.

_____ Flight hardware, which with minor modifications will be suitable for use on Spacelab/LDEF, is being or has been developed for use on (program name) _____

_____

Investigation Title _____

_____

_____ Flight hardware from existing inventory of instruments.

_____ Other, describe _____
_____
_____

C. Please list any potential problems or other areas of uncertainty with regard to the instrumentation, its interfacing to Spacelab, and its operation in the Spacelab environment. Final thermal interface cannot be completed until mission flight profile and orientation in orbiter bay are known. Mechanical interface requires definition as to mounting configuration on IPS.

D. Please estimate the time you would require, after selection and funding, before your flight instrument could be delivered for integration into Spacelab/LDEF. Show approximately how this time would be apportioned between the three phases listed below:

Definition	6	months
Design and Fabrication	30	months*
Test	2	months

*Procurement Cycle after Selection is 10-12 months additional

IF YOUR INVESTIGATION IS PROPOSED FOR LDEF, COMPLETE SECTION III AND DISREGARD THE REMAINING SECTION. OTHERWISE, OMIT THIS SECTION AND PROCEED.

III. REQUIREMENTS FOR LDEF

A. Minimum and maximum limits on flight duration required to achieve the investigation objectives _____ to _____ months.

B. Range of orbit parameters compatible with your investigation

   Attitude _____ to _____ km

   Inclination _____ to _____ deg

C. Physical characteristics of Instrumentation

   Amount of tray space _____ tray.

   Tray depth require _____ in.

   If instrument cannot be accommodated in a standard tray, attach a dimensioned sketch or drawing of the package.

   Instrument weight _____ kg

D. Describe any restrictions on the package surface which might affect thermal control. _____
   _____
   _____
   _____
   _____

E. Maximum 10-minute average power dissipation in package _____ watts

F. Contamination - Describe any environmental factors, such as particle radiation, RF radiation, magnetic fields, etc., which would adversely affect your instrument as well as any contamination your instrument can produce which might influence other instruments. _____

_____

_____

_____

IV. REQUIRED SPACELAB MISSION CHARACTERISTICS

A. The major Spacelab elements, long and short pressurized modules, and pallets can be arranged in various flight configurations such as module only, module with pallet(s), and pallets only. Describe briefly any restrictions on the flight configuration required to accommodate your instrumentation. ___None_____

_____

_____

_____

B. The standard Spacelab flight duration of 7 days can be extended to 30 days if the necessary provisions are added. Indicate the minimum duration required to achieve your objectives. __5 days*_____
If flights longer than 7 days are detrimental, please indicate the nature of the problem and the maximum allowable flight duration.

* Flare studies and studies of active region evolution may require additional time for targets of opportunity to appear. Extensions to flight durations of 30 days would be highly desireable in assuring that data on many types of transient solar phenomena were obtained.

C. Epoch/Orbit/Attitude

Range of orbit parameters compatible with your investigation

Attitude ____220____ to ___600____ km

Inclination ___28____ to _58____ deg

If your investigation requirements impose constraints on the mission epoch or orientation of the orbit or spacecraft (i.e., solar viewing,

viewing sunlit Earth targets, wintertime viewing of arctic auroral zone, etc), please describe these requirements. <u>Solar</u> <u>viewing is required.</u>

V. FLIGHT INSTRUMENT CHARACTERISTICS AND REQUIREMENTS

A. Estimated mission resources required in orbit to achieve objectives

1. Launch mass (includes all instrument, instrument peculiar equipment and consumables) <u>127.57</u> kg. (Addition of an offset point system would add 38.42 kg.

2. Total electrical energy <u>14.9 K</u> watt-hours.

3. Total digital data downlinked <u>60000</u> megabits. *
   *Primarily for AID detector on last 2 days of 1st mission

4. Total crew time <u>about 4</u> man-hours. (instrument set-up time, in 15 minute blocks)

5. Total observation time <u>40</u> hours.

B. Please provide brief, one or two sentence descriptions, of each of the instrument modes.
<u>Prime mode: Photographic spectra using either a narrow entrance slit (line profile or diagnostics mode), a wide slit (wide-field or flare mode) or a combination of the above (combination mode); H alpha slit jaw video monitor for target selection.</u>

<u>Secondary mode: Photoelectric imaging detector, time sharing its output line with H alpha slit jaw video monitor.</u>

Please estimate the following parameters for each major operating mode of your instrument. Include on-orbit standby mode if it requires power or data channels.

| Parameter | EUV CAMER | | | AID | STANDBY |
	Mode 1 diagnostics mode	2 flare mode	3 combination mode	4	5
Power (watts)					
28 V Bus	163.55	163.55	163.55	170.05	112[1]
400 Hz Bus	---	---	---	---	---

(1) includes 50 w heater power for all modes

Parameter	EUV CAMER			AID	STANDBY
Digital Data Downlink Rate (bits/sec)	1.28 Mbps for one second every 10 sec. or 128 kbps for digital video			1.28 Mbps	1 kbps
Analog Data (Downlink) Bandpass (kHz)					
Video Downlink Required (Yes or No)	yes--either could multiplex in analog form (one frame per second) or send down digitally				
Typical duration of mode (minutes)	60 min	60 min	60 min	60 min	
Number of cycles of mode required to achieve objectives	10	5[2]	15	10	

(2) Flare alert standby time (10-20 hours) highly desirable

C. Please identify and provide accuracy of all ancillary parameters required from sources external to your instrumentation onboard real-time operations and for post-mission data analysis:

Parameter	Onboard	Post-Mission
Absolute Time, UTC (millisec)	1 sec	1 sec
Orbiter Position (meters)	not needed	not critical
Orbiter Velocity (m/sec)	not needed	not critical
Orbiter Attitude (deg)	not needed	not critical
Other (describe)		

D. Instrument Package Description Sheet

The number of separately mounted packages comprising your instrumentation is ___1___ (can be divided into two [electronics package separate] if required for thermal control.)
For each package please fill out an Instrument Package Description Sheet as shown on following page (extra copies of this sheet are appended to this document).

Instrument Package Description Sheet

1. **Package ID Number** _____1_____   2. **Weight (kg)** _127.57_

3. **Package Location, i.e., AFT Flight Deck, Pressurized Module, Pallet, Spacelab Instrument Pointing System, Other (describe).**
   Mounted on Space lab Instrument Pointing System or other
   pointing system

4. **Thermal Control Information**

   a. Temperature Limits ($^\circ$C)

Operating	16	to	24
Standby (on orbit)	-10	to	28

   b. Maximum 10-minute average power dissipation (watts)
   _68.33_

   c. Restrictions on package surface which could affect thermal control (conducting surface, apertures, etc.) Aperture of about 140 cm^2 on end facing sun. Package requires mounting brackets to IPS

5. **Power Required (watts)**

Instrument Op. Mode	1	2	3	4	5
28 V S/L Bus	163.55	163.55	163.55	170.05	112
400 Hz S/L Bus	none				

6. **Please provide brief functional description of package:** Optics focus visible and EUV radiation on an entrance aperture which admits a portion of the solar EUV image to illuminate a toroidal grating. The dispersed EUV radiation is focussed on film for a permanent record (to be developed later). An H alpha slit jaw camera monitors the scene around the entrance aperture. Photoelectric image detection is also planned.

7. **Provide a dimensional sketch of package showing size and shape, location of center of gravity, mounting arrangement, and any field-of-view requirements.** (See Fig. 1)

8. **Does package have any rotating parts?** (Yes, No) film spool rotation during camera film advance

9. **As appropriate, describe contamination sensitivity requirements, sources of contamination (magnetic, RF, outgassing, radioactivity, etc.) deployment requirements, etc.**
   Package incorporates external door for environmental protection. It will not produce contamination. A weak (about 1 microcurie) radioactive source of Fe^{55} emitting x-rays may be incorporated for calibration purposes. X-radiation will not penetrate case of instrument.

E. **Instrument Control**

1. Please indicate applicable flight control requirement.

    _____ **None required**

    _____ **Requires only predefined and scheduled commands**

    __X__ **Requires real-time interactive control (observation of data, decisions, adjustments of instrument, etc.)** for initiation of prestored data sequences.

2. If interactive control is required, please indicate the applicable method(s).

    __X__ By onboard crew (real time)

    __X__ By ground crew (near-real time)

3. Commands

    a. Total number of discrete command lines required __46__.

    b. Estimated total number of discrete commands required during flight operations _____80_____.

    c. Estimated total number of serial bits to be sent to instrument by Spacelab C&DH system during flight operations __10,000 max.__
       2560 min.

F. **Instrument Pointing**

1. Does your investigation require instrument pointing?

    __X__ Yes; _____ No. if "No," skip balance of this section.

2. Pointing will be provided by:

_____ The Orbiter orientation

_____ The instrument

__X__ A NASA - provided pointing system

_____ Other, describe _____

_____

_____

_____

_____

3. Pointing accuracy required _____10_____ __arcsec__ .
                                                    units*

4. Pointing stability _____1_____ arcsec (1σ) for _____10_____
   minutes.   units*
(Will produce 50% deterioration in spatial resolution. 0.3 arcsec (1σ)
will produce 5% deterioration). Inhibition of thruster firings is desirable.
   5. Accuracy with which pointing direction must be known _____1_____

   __arcsec__
     units*

6. Describe any other important aspects of the pointing requirements.
1. Pointing direction should be changeable in 20 arcsec increments in the
direction normal to the slit length by command from the SEUTS after each set
of exposures is complete (to build up spectroheliograms); 2. Roll of IPS to
be specified and set to 1° accuracy for special observing programs; 3. Off-
set pointing to specified coordinates required; 4. Capability of co-align-
ment with other solar instruments would enhance scientific results of mission.

VI.   SPECIAL SUPPORT REQUIREMENTS

Please describe all special support required for each of the following three
phases:

A. Integration and launch preparations (Cryogenic loading, Calibration,
   clean room, ground access, etc.) 15 watts power are requested prior
   to and during launch to maintain command load in microprocessor.
   Access to load flight film within 1 week of launch is required;
   Ambient temperature to be 25°C or less after loading.
*Indicate angle units, i.e., deg, arc-min, arc-sec, etc.

B. Flight operations, both onboard and ground. (Crew EVA, RMS manipulation, real-time data processing and display at POCC, etc.). _____

Crew operations at AFD: 15 blocks of 15 minutes each to locate targets via H-alpha monitor and initiate observing sequences; 15 blocks of command control of IPS from ground to initiate sequences on targets displayed on video monitor data from previous orbit (followed by remainder of each orbit for observations).

C. Orbiter landing (film or instrument removal, etc.). Instrument must be cooled below 25°C as quickly as possible after landing using ground purge system.

D. Orbital Environment. Active thermal protection using GRT-4 Thermal Canister or equivalent, if available, is highly desirable.

VII FLIGHT SYSTEM SAFETY

Attachment C3 of this AO describes the safety policy and requirements applicable to all Space Transportation System payloads. Please list those elements of your instrumentation and its operation which will require study and documentation in the Safety Assessment Report.
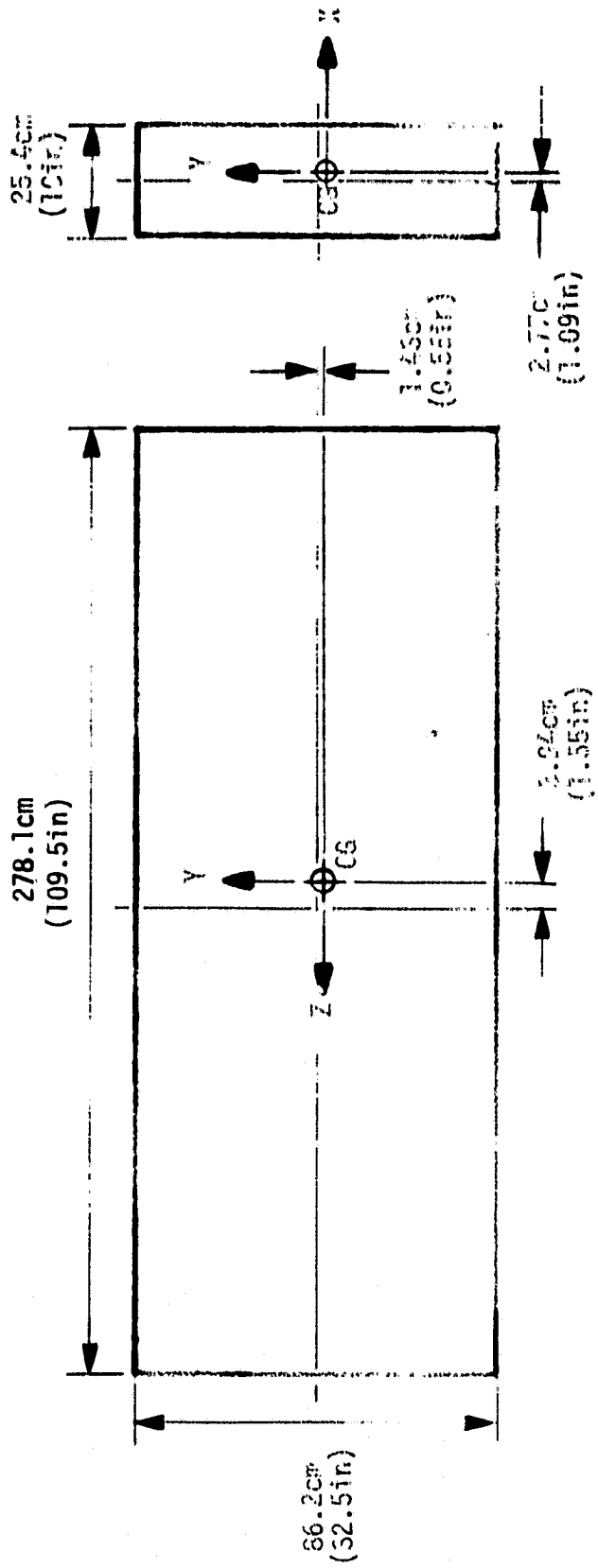
None known at this time

FIGURE 1